Aus der

Klinik und Poliklinik für Frauenheilkunde und Geburtshilfe

Klinik der Universität München

Direktor: Prof. Dr. Sven Mahner

Die Rolle der Nekroptose im Zervixkarzinom und ihre Assoziation mit dem klinischen Verlauf

Dissertation
zum Erwerb des Doktorgrades der Medizin
an der Medizinischen Fakultät
der Ludwig-Maximilians-Universität zu München

vorgelegt von
Tilman Lauritz Rüdiger Vogelsang

aus
Göttingen

2025

Mit Genehmigung der Medizinischen Fakultät
der Universität München

Berichterstatter:	Prof. Dr. Udo Jeschke
Mitberichterstatter:	Prof. Dr. Doris Mayr
	Prof. Dr. Enrico De Toni
	Prof. Dr. Nicole Terpolilli
Mitbetreuung durch den promovierten Mitarbeiter:	PD Dr. Aurelia Vattai
Dekan:	Prof. Dr. med. Thomas Gudermann
Tag der mündlichen Prüfung:	13.11.2025

Affidavit

Eidesstattliche Versicherung

Vogelsang, Tilman Lauritz Rüdiger

Name, Vorname

Ich erkläre hiermit an Eides statt, dass ich die vorliegende Dissertation mit dem Titel:

Die Rolle der Nekroptose im Zervixkarzinom und ihre Assoziation mit dem klinischen Verlauf

selbständig verfasst, mich außer der angegebenen keiner weiteren Hilfsmittel bedient und alle Erkenntnisse, die aus dem Schrifttum ganz oder annähernd übernommen sind, als solche kenntlich gemacht und nach ihrer Herkunft unter Bezeichnung der Fundstelle einzeln nachgewiesen habe.

Ich erkläre des Weiteren, dass die hier vorgelegte Dissertation nicht in gleicher oder in ähnlicher Form bei einer anderen Stelle zur Erlangung eines akademischen Grades eingereicht wurde.

Graz, 16.11.2025 — Tilman Lauritz Rüdiger Vogelsang

Ort, Datum — Unterschrift Doktorand

Inhaltsverzeichnis

Abkürzungsverzeichnis

TMA	tissue micro array
IRS	Immunoreaktiver Score
MTT	3-(4,5-Dimethylthiazol-2-yl)-2,5-diphenyltetrazoliumbromid
BrdU	Bromdesoxyuridin
hr-HPV	high-risk human papillomavirus
UICC	Union International contre le cancer
FIGO	Fédération Internationale de Gynécologie et d'Obstétrique
ZBP1	Z-DNA binding protein
RIPK3	receptor-interacting serine/threonine-protein kinase 3
MLKL	mixed lineage kinase domain like protein
pMLKL	phosphorylated mixed lineage kinase domain like protein
DAMPs	damage associated molecular patterns
TNFα	tumor necrosis factor α
TNFR1	tumor necrosis factor receptor 1
RIPK1	receptor-interacting serine/threonine-protein kinase 1
$cFLIP_L$	cellular FLICE-like inhibitor protein long isoform
Casp8	Caspase 8
Cyld	cylindromatosis
cIAP1/2	cellular inhibitor of apoptosis protein 1 and 2
$cFLIP_S$	cFLIP short isoform
HSP	heat shock protein
CDC37	cell division cycle 37

Publikationsliste

Folgende Publikationen stellen die Grundlage für diese kumulative Dissertation dar:

Publikation I

RIPK1 and RIPK3 are positive prognosticators for cervical cancer patients and C2 ceramide can inhibit tumor cell proliferation *in vitro*.

Vogelsang TLR, Kast V, Bagnjuk K, Eubler K, Jeevanandan SP, Schmoeckel E, Trebo A, Topalov NE, Mahner S, Mayr D, Mayerhofer A, Jeschke U, Vattai A.

Front Oncol. 2023 May 1; 13:1110939.

doi: 10.3389/fonc.2023.1110939

Publikation II

Prognostic Impact of Heat Shock Protein 90 Expression in Women Diagnosed with Cervical Cancer.

Vogelsang TLR, Schmoeckel E, Topalov NE, Ganster F, Mahner S, Jeschke U, Vattai A.

Int J Mol Sci. 2024 Jan 26; 25(3):1571.

doi: 10.3390/ijms25031571

Zusätzlich wurden basierend auf der experimentellen Arbeit folgende Originalarbeiten publiziert:

Regulation of LCoR and RIP140 expression in cervical intraepithelial neoplasia and correlation with CIN progression and dedifferentiation.

Vogelsang TLR, Schmoeckel E, Kuhn C, Blankenstein T, Temelkov M, Heidegger H, Kolben TM, Kolben T, Mahner S, Mayr D, Jeschke U, Vattai A.

J Cancer Res Clin Oncol. 2020 Jul;146(7):1847-1855.

doi: 10.1007/s00432-020-03178-x

Trace Amine-Associated Receptor 1 (TAAR1) Is a Positive Prognosticator for Epithelial Ovarian Cancer.

Vogelsang TLR, Vattai A, Schmoeckel E, Kaltofen T, Chelariu-Raicu A, Zheng M, Mahner S, Mayr D, Jeschke U, Trillsch F.

Int J Mol Sci. 2021 Aug 6;22(16):8479.

doi: 10.3390/ijms22168479

1. Beitrag zu den Publikationen

1.1 Beitrag zu Publikation I

"RIPK1 and RIPK3 are positive prognosticators for cervical cancer patients and C2 ceramide can inhibit tumor cell proliferation in vitro"

Der Ethikantrag für die vorliegende Publikation war bereits durch die Betreuerin PD Dr. Aurelia Vattai gestellt und durch die Ethikkommission der Ludwig-Maximilians-Universität München bewilligt worden (Ethikvotum mit Approval Number 259-16, 2016). Da diese Dissertation im Rahmen des strukturierten Promotionsprogramms „Förderung für Forschung und Lehre (FöFoLe)" erfolgte, bestand bereits ein Plan über das Forschungsvorhaben und den Umfang dieser Arbeit. Im Verlauf wurde dieser Plan durch mich in Zusammenarbeit mit PD Dr. Vattai und Prof. Dr. Jeschke adaptiert.

Das untersuchte Patientinnenkollektiv umfasste 250 Zervixkarzinompatientinnen. Dies war bereits etabliert und wurde mit aktuellen Daten des Tumorregisters München sowie Daten aus den Archiven der Frauenklinik der LMU München durch mich ergänzt. Die Tumorblöcke der 250 Patientinnen wurden von mir aus dem Archiv herausgesucht, markiert und in das Institut für Pathologie der Ludwig-Maximilians-Universität München transportiert, wo aus den Blöcken von einer geschulten pathologischen MTA Tissue Micro Arrays (TMAs) angefertigt und geschnitten wurden. Diese Schnitte stellen die Grundlage für beide Publikationen dar. Das Material wurde von mir gefärbt und mittels Immunoreaktivem Score [1] ausgewertet. Die Zellversuche (MTT, BrdU, Live Cell Imaging, Western Blot, Flow Cytometry) wurden von Prof. Dr. Udo Jeschke, PD Dr. Aurelia Vattai, Konstantin Bagnjuk, Verena Kast, Katja Eubler und mir entworfen. MTT (3-(4,5-Dimethylthiazol-2-yl)-2,5-diphenyltetrazoliumbromid) und BrdU (Bromdesoxyuridin) wurden von mir durchgeführt. Nach Einführung in das Statistikprogramm „SPSS" durch Prof. Dr. Udo Jeschke erfolgten alle statistischen Auswertungen durch mich. Das gesamte Manuskript, alle Tabellen und Graphen inklusive Fotos wurden von mir erstellt. Abschließend wurde das Manuskript durch PD Dr. Aurelia Vattai, Prof. Dr. Udo Jeschke sowie durch die weiteren Ko-Autoren evaluiert. Der Reviewprozess wurde in Rücksprache mit PD Dr. Aurelia Vattai, Prof. Dr. Artur Mayerhofer und Prof. Dr. Udo Jeschke durch mich geleitet.

1.2 Beitrag zu Publikation II

“Prognostic Impact of Heat Shock Protein 90 Expression in Women Diagnosed with Cervical Cancer”

Als Grundlage für dieses Paper diente ebenfalls das oben erwähnte und etablierte Kollektiv. Die immunhistochemische Färbung der TMAs, die Auswertung mittels IRS sowie die statistische Auswertung mittels Kruskal–Wallis-H test, log-rank (Mantel–Cox) und Cox regression Tests wurden von mir durchgeführt.

Ich verfasste das gesamte Manuskript selbstständig und erstellte alle darin enthaltenen Tabellen, Graphen und Fotos. Anschließend wurde das Manuskript durch PD Dr. Aurelia Vattai, Prof. Dr. Udo Jeschke sowie durch die weiteren Ko-Autoren evaluiert. Der Reviewprozess wurde in Rücksprache mit PD Dr. Aurelia Vattai und Prof. Dr. Udo Jeschke durch mich geleitet.

2. Einleitung

2.1 Zervixkarzinom

2.1.1 Epidemiologie

Das Zervixkarzinom stellt mit 660 000 neuen Fällen und 350 000 Todesfällen im Jahr 2022 nach dem Mamma-, dem Bronchial- und dem kolorektalen Karzinom das weltweit vierthäufigste Karzinom bei Frauen dar [2]. Im Laufe der letzten Jahrzehnte konnte die hohe Inzidenzrate durch effektive Screenings, wie dem zytologischen Abstrich nach Papanicolaou, und Verbesserungen der Behandlungsmöglichkeiten deutlich reduziert werden [3, 4]. Dieser Trend lässt sich vorwiegend in westlichen Staaten mit organisierten Screeningmethoden beobachten. Es herrschen, abhängig vom Zugang zu Screening, Impfung und Behandlungsmöglichkeiten, große regionale Differenzen. So ist die Inzidenz der diagnostizierten Zervixkarzinome in Staaten der Subsahara am höchsten [2, 5-8]. In Deutschland beträgt die 5-Jahres-Überlebensrate nach Erstdiagnose eines invasiven Zervixkarzinoms 64% [9].

Bei Erstdiagnose des Zervixkarzinoms beträgt das mittlere Alter 53 Jahre, mit einem Altersgipfel zwischen 40 bis 59 Jahren [3, 9]. Damit hat sich das mittlere Alter bei Erstdiagnose in den letzten 25 Jahren um mehr als 15 Jahre verringert [3].

2.1.2 Histologie, Ätiologie und Onkogenese

Histopathologisch ist das Zervixkarzinom mit 80% meist epithelialen Ursprungs. In 20% handelt es sich um ein Adenokarzinom. Seltene Tumorentitäten sind adenosquamöse, neuroendokrine oder klarzellige bzw. serös-papilläre Zervixkarzinome [3].

Die Ätiologie des Zervixkarzinoms stellt in den meisten Fällen eine persistierende Infektion mit einem der high-risk humanen Papillomaviren (hr-HPV) dar [10]. HPV-negative Zervixkarzinome sind mit 3-8% aller Zervixkarzinome selten und haben eine schlechtere Prognose [11]. Die häufigsten hr-HPV-Typen sind HPV-Typ 16 und 18. Eine persistierende Infektion kommt in nur etwa 5-10% aller Infektionen vor, wobei 3% aller infizierten Frauen an einem Zervixkarzinom erkranken [3, 12].

Auf molekularer Ebene führt eine persistierende Infektion durch Degradierung und Inaktivierung von p53 und dem Retinoblastom-Protein durch die viralen Onkoproteine E6 und E7 zur Störung des Zellzyklus, zur genomischen Instabilität und Hyperproliferation. Des Weiteren blockieren die Onkoproteine E6 und E7 die Apoptose und stärken so Immortilitätsbestrebungen [4, 13].

Neben einer persistierenden HPV-Infektion mit den high-risk Typen 16 und 18 stellen Rauchen, Immunsuppression und häufig wechselnde Geschlechtspartner Risikofaktoren für die Entstehung eines Zervixkarzinoms dar [14, 15].

2.1.3 Klinik, Diagnostik und Staging

In den frühen Stadien präsentiert sich das Zervixkarzinom meist asymptomatisch. Bei fortgeschrittener Erkrankung können sich vaginale Blutungen (beispielsweise als azyklische Blutung oder Kontaktblutung nach Kohabitation), übelriechender Fluor, Hydronephrose infolge von Ureterstenose, Lymphödem, von lumbosakral in den Unterbauch ausstrahlende Schmerzen sowie Miktions- bzw. Defäkationsbeschwerden zeigen [16, 17].

Neben einer ausführlichen Anamnese (Symptomatik, Sexualanamnese, Nikotinabusus, Zeitpunkt sowie Ergebnis der letzten Vorsorgeuntersuchung) und der vaginalen Palpation stellt die Spekulumeinstellung zur makroskopischen Beurteilung der Portio vaginalis uteri einen Bestandteil der Diagnositk dar. Die Diagnose des Zervixkarzinoms wird bei auffälliger Differentialkolposkopie (und/oder auffälligem PAP-Abstrich) histologisch anhand einer Biopsie aus der Portio gesichert. Auch die bildgebende Diagnostik soll stadienabhängig implementiert werden [3, 17].

Zur Stadieneinteilung soll laut aktuellen Leitlinien die TNM-Klassifikation des Union International contre le cancer (UICC) von 2010 verwendet werden. Optional kann die kongruente Fédération Internationale de Gynécologie et d'Obstrétique (FIGO)-Klassifikation angewandt werden [3, 18].

2.1.4 Therapie und Prävention

Die primäre Therapie besteht zumeist aus operativem oder radio(chemo)therapeutischem Ansatz abhängig vom Tumorstadium nach FIGO. Besonders in Frühstadien (IA bis IIA) wird im deutschsprachigen Raum der unimodale Therapieansatz mittels Operation bevorzugt [3]. Die primäre operative Therapie erfolgt nach der Piver-Rutledge-Klassifikation, bei welcher nach Ausmaß der radikalen Hysterektomie klassifiziert wird [3, 19]. Bei Lymphknotenbefall, Inoperabilität oder bei ausgedehnten Tumorstadien (≥ Stadium IIB) wird die primäre Radio(chemo)therapie angewandt. Die Histopathologie (Adenokarzinom, Plattenepithelkarzinom) spielt bei der Therapieentscheidung eine untergeordnete Rolle [3].

Seit 2007 besteht die STIKO-Empfehlung, Mädchen und junge Frauen vor der Kohabitarche gegen HPV impfen zu lassen [20]. Auch für Jungen und junge Männer gilt diese

Empfehlung seit 2018 [21]. Die aktuell zugelassenen Impfstoffe sind bivalent beziehungsweise nonavalent und zeigen einen präventiven Effekt vor Infektionen mit den häufigsten onkogenen HPV-Stämmen (u.a. HPV-Typ 16 und 18). Die systematische Implementierung der HPV-Impfung (bspw. als Schulimpfprojekt) kann zu einer erhöhten Impfrate und somit langfristig zu einer weiteren Reduktion der Inzidenz führen [3, 22-26].

2.2 Programmierter Zelltod und HPV

Der Zelltod ist essenzieller Bestandteil irdischen Lebens [27]. Die bekanntesten und am besten erforschten Formen des Zelltodes sind Nekrose und Apoptose. Während Nekrose häufig durch chemische, physikalische oder biologische Noxen ausgelöst wird, stellt die Apoptose eine Form des programmierten Zelltods dar. Typischerweise führt die Nekrose zu einer inflammatorischen Reaktion, wohingegen die Apoptose immunologisch silent abläuft. Neben diesen existieren noch viele weitere Formen des Zelltods, wie beispielsweise NETose, Pyroptose oder Nekroptose [28].

Diese Arbeiten beschäftigen sich mit der Nekroptose, einer Form des programmierten Zelltodes, welche durch Signalkaskaden stark reguliert ist aber ungleich zur Apoptose zu einer Entzündungsreaktion führt und Caspasen-unabhängig stattfinden kann [4, 6, 28].

2.2.1 Nekroptose

Diese Form des programmierten Zelltodes führt Caspase-unabhängig zu einer lokal-entzündlichen Reaktion [4, 28]. Die viralen Onkoproteine high-risk E6 und high-risk E7 stören den Zellzyklus und beeinflussen Regulatoren der Zellproliferation, Apoptose, Zellimmortilisierung und Chromosomenstabilität [13]. High-risk E7 bindet das Retinoblastom-Protein und führt zu dessen Abbau. Durch die Unterbrechung der Bindung zwischen pRb und E2F, einem wichtigen Regulator des Zellzykus, kommt es zur Hyperproliferation [29, 30]. High-risk E6 bindet das zelluläre E6 ubiquitin ligase E6 associated protein. Dieser Komplex führt zum Abbau von p53 und blockiert dadurch die Apoptose, führt zur genomischen Instabilität und begünstigt Mutationen [13, 31-33].

Ausgelöst wird die Nekroptose durch unterschiedliche Mechanismen. Eine Möglichkeit stellt die Aktivierung des Z-DNA binding proteins (ZBP1) dar [28]. Z-DNA ist eine Form der DNA, die durch Torsionsspannung bei schneller DNA-Synthese entsteht. Dies findet beispielsweise bei viraler Infektion der Zelle statt. Durch die Bindung an Z-DNA oder Z-RNA wird ZBP1 aktiviert [28]. ZBP1 bindet receptor interacting serine/threonine-protein kinase 3 (RIPK3) [34]. Diese Interaktion fördert die Autophosphorylierung von

RIPK3 und führt anschließend zur Bindung und Aktivierung von mixed lineage kinase domain like pseudokinase (MLKL). Dadurch wird MLKL zu pMLKL phosphoryliert und aktiviert [28, 35]. Der RIPK3-MLKL Komplex wird als zentraler Mediator der Nekroptose gesehen [36]. pMLKL formt ein Oligomer und bindet an Lipide der inneren Zellmembran, was zur Bildung einer nekroptotischen Pore und der Unterbrechung der Integrität der Zellmembran führt [37]. Die anschließende Freisetzung von damage associated molecular patterns (DAMPs) führen zur intensiven Aktivierung des Immunsystems [38].

Der komplexere Weg der Aktivierung der Nekroptose wird durch Bindung von tumor necrosis factor α (TNFα) an den tumor necrosis factor receptor 1 (TNFR1) initiiert [28]. Diese Bindung führt zu Polyubiquitinylierung von receptor interacting serine/threonine-protein kinase 1 (RIPK1) [39] und letztlich zur Hochregulierung von anti-apoptotischer Genexpression wie beispielsweise A20 und das cellular FLICE-like inhibitor protein long isoform (cFLIPL) [28, 40-42]. Caspase 8 (Casp8)- cFLIPL heterodimere inhibieren nicht nur die Apoptose [43], sondern verhindern auch die Nekroptose durch Aufspaltung von RIPK3 [44], RIPKP1 [45] und der Deubiquitinase cylindromatosis (Cyld) durch dauerhafte basale katalytische Aktivität [42, 46]. Bei nicht vorhandener Polyubiquitinylierung von RIPK1 (z.B. bei Abwesenheit von cellular inhibitor of apoptosis protein 1 and 2 (cIAP1/2) oder durch Deubiquitinylierung durch Cyld) wird Zelltod induziert [28, 47-49]. Insuffiziente Spiegel an cFLIPL oder cFLIP short isoform (cFLIPS) führen zur Autokatalysierung und Aktivierung von Casp8 und somit zur Induktion der Apoptose [47]. Bei einem adäquat vorliegenden RIPK3-Spiegel blockiert ein gesteigerter cFLIPL-Spiegel die Nekroptose, wohingegen gesteigerte cFLIPS-Spiegel durch Inhibierung von Casp8 zur Induktion der Nekroptose führen [47]. Nekroptose kann nur stattfinden, wenn Caspasen inaktiviert oder abgebaut sind [48]. Dann kann es zur Aktivierung von RIPK1 kommen, welches einen Komplex mit RIPK3 eingeht, dem sogenannten Nekrosom oder RIPK1-RIPK3-Komplex [47, 48]. Nach dessen Aktivierung oligomerisiert RIPK3 und formt einen Komplex mit MLKL. Dies führt zur Phosphorylierung von MLKL zu pMLKL und zur Bildung einer nekroptotischen Pore, der Unterbrechung der Integrität der Zellmembran und der Freisetzung von DAMPs [36-38].

2.2.2 Ceramide

Sphingolipide sind Lipide, die eine zentrale Rolle bei Inflammation, Zellproliferation und Zelltod spielen [50]. Auch bei der Kanzerogenese sind biologisch aktive Sphingolipide, zu welchen auch Ceramide gehören, relevant [51]. In Neuroblastom- und Brust-

karzinomzellen haben Ceramide durch die Induktion von Apoptose einen tumorsuppresiven Effekt [4, 52, 53]. In humanen lutealen Granulosazellen konnte mittels C2 Ceramid die Nekroptose ausgelöst werden [54].

2.2.3 Heat Shock Protein 90

Heat Shock Protein 90 (HSP90) und das Co-Chaperon cell division cycle 37 (CDC37) werden während der Nekroptose benötigt, um RIPK3 zu aktivieren [55]. Hemmung oder Abbau von HSP90 führt zur Inhibition von Nekroptose durch Abbau der für die Nekroptose essenziellen Proteine RIPK1, RIPK3 und MLKL [6, 56-59].

Chaperone „überwachen" die Proteinfaltung und dienen der Proteostase (= Protein-Homeostase) [60]. Wenn die Zelle Situationen wie beispielsweise einem plötzlichen Temperaturanstieg ausgesetzt ist, steigt die Expression von Chaperonen, daher die Bezeichnung „Heat Shock Protein" [61]. Probleme bei der Proteostase können sowohl zur Manifestation als auch dem Progress von neurodegenerativen, neoplastischen und kardiovaskulären Erkrankungen sowie Demenz führen [60]. Somit stellen Chaperone ein vielversprechendes Target für diverse Therapieansätze dar. Strukturiert werden Chaperone anhand ihres molekularen Gewichts (HSP40, HSP60, HSP70 HSP90, HSP100 und kleine HSPs) [60].

HSP90 hat mit mehreren Hundert Substraten wichtige und vielseitige Aufgaben in Stress- als auch physiologischen Situationen einer eukaryoten Zelle. Dieses Chaperon spielt eine essenzielle Rolle in der Proteinfaltung, bei programmiertem Zelltod, bei DNA-Reparaturprozessen und bei immunreaktiven Prozessen [6, 61, 62].

2.3 Zielsetzung der Arbeit

Die Kanzerogenese des Zervixkarzinoms beruht in den meisten Fällen auf einer persistierenden Infektion mit HPV [4, 10]. Die Inhibition der Nekroptose mittels Herabregulation von RIPK3, einem zentralen Protein in der nekroptotischen Signalkaskade, ermöglicht hr-HPV, in Teilen den immunologischen Abwehrprozessen auszuweichen und somit möglicherweise den Progress hr-HPV induzierter Läsionen zu fördern [4, 63].

Der Fokus der ersten Publikation ist, das klinische Outcome von Patientinnen mit diagnostiziertem Zervixkarzinom mit der Expression der Schlüsselfaktoren der nekroptotischen Signalkaskade zu korrelieren (RIPK1, RIPK3 und pMLKL). Mittels statistischer Überlebens- und Korrelationsanalysen wird deren Potential eines unabhängigen, prognostischen Markers bei Patientinnen mit Zervixkarzinom evaluiert. Anschließend soll in Zellversuchen Nekroptose in Zervixkarzinomzelllinien ausgelöst werden. Hierfür wird

mit C2 Cermid eine Substanz verwendet, welche in einer vorausgegangenen Publikation der kooperierenden Arbeitsgruppe von Prof. Mayerhofer Nekroptose in lutealen Granulosazellen ausgelöst hat [4, 54].

Da HSP90 im Rahmen der Nekroptose für die Aktivierung von RIPK3 einen wichtigen Faktor darstellt [55] und eine Inhibierung von HSP90 zur Hemmung der Nekroptose führt [56-59], steht die Korrelation des klinischen Outcomes mit der Expression von HSP90 im Zervixkarzinom im Mittelpunkt der zweiten Publikation. Hiermit soll ermittelt werden, ob HSP90 als unabhängiger prognostischer Marker bei Patientinnen mit Zervixkarzinom fungieren kann [6].

3. Zusammenfassung

Das Zervixkarzinom stellt trotz deutlichem Rückgang der Inzidenz im Laufe der letzten Jahrzehnte eine der häufigsten Tumorentitäten bei Frauen dar. In einem Großteil der Fälle wird das Zervixkarzinom durch high-risk HPV-Stämme verursacht. Pathophysiologisch führt eine Infektion der Zelle mit einem hr-HPV Stamm zur Störung des Zellzyklus, der Verstärkung der genomischen Instabilität, Hyperproliferation sowie Hemmung der programmierten Zelltodformen Apoptose und Nekroptose. Die Hemmung der Nekroptose geschieht durch die Herabregulierung der Expression von RIPK3. Durch die Ergebnisse dieser Dissertation konnte gezeigt werden, dass Patientinnen, die an einem Zervixkarzinom leiden, ein besseres klinisches Outcome zeigen, wenn Proteine der nekroptotischen Signalkaskade (RIPK1, RIPK3, pMLKL) vermehrt exprimiert werden. Des Weiteren konnte gezeigt werden, dass das Chaperon HSP90, welches unter anderem für die Proteinfaltung der Nekroptoseproteine essenziell ist, ebenfalls als positiv prognostischer Faktor gesehen werden kann.

Mittels eines Ceramids (C2 Ceramid) wurde in der ersten Arbeit versucht, die Nekroptose in den drei Zervixkarzinomzelllinien CaSki, HeLa und SiHa zu induzieren. Hierbei konnten bei CaSki- und HeLa-Zellen die für die Nekroptose typischen morphologischen Veränderungen wie Verlust der Konfluenz und „ballooning“ der Zellen gesehen werden.

Diese Ergebnisse lassen die Nekroptose, welche aufgrund der einhergehenden inflammatorischen Immunreaktion besonders im kardiovaskulären Bereich als unwillkommene Zelltodform gesehen wird, in einem anderen Licht erscheinen.

Nachdem anhand der Ergebnisse dieser Arbeit eine prognostische Relevanz der Schlüsselfaktoren der nekroptotischen Signalkaskade abzuleiten ist, bedarf es in der Folge experimentelle Studien, welche die Nekroptose als potenzielles therapeutisches Target sehen. Hierbei könnte insbesondere der Unterschied des proliferations- und viabilitätshemmenden Effekts des isolierten Auslösens der Nekroptose zum isolierten Auslösen der Apoptose von Interesse sein. Dadurch kann die Bedeutung der Nekroptose als Backup Mechanismus bei Hemmung der Apoptose durch HPV weiter erläutert werden.

4. Abstract

Despite a decline of incidence in cervical carcinoma within the past decades, it remains the 4th most common cancer in females. In most cases, cervical carcinoma is caused by high-risk human papilloma virus. Besides disturbing the cell cycle, promotion of genomic instability and hyperproliferation, high-risk human papillomavirus inhibits apoptosis as well as necroptosis. We hypothesized that women who have a higher expression of proteins essential for necroptosis (RIPK1, RIPK3 and pMLKL) have a better clinical outcome including overall survival and progressive free survival. This doctoral thesis showed that there is a positive correlation between higher expression of RIPK1, RIPK3 and pMLKL and key clinical outcomes. Furthermore, we examined heat shock protein 90 which functions as a chaperone for the proteins essential for necroptosis. We could show that HSP90 is a positive prognosticator for OS and PFS in cervical squamous cell carcinoma patients.

In cell culture experiments, we examined the effect of C2 ceramide on the three cervical cancer cell lines CaSki, HeLa and SiHa. In CaSki and HeLa cells we could show that C2 ceramide leads to morphological changes typical for necroptosis, such as loss of confluency and "ballooning".

Due to the inflammatory response, necroptosis is often seen as a negative process, especially in cardiovascular diseases. This work enlightens a different, positive impact of necroptosis.

More studies will be needed to further characterize the specific microbiological mechanism and to implement necroptosis as a possible therapeutic target.

5. Publikation I

Titel

RIPK1 and RIPK3 are positive prognosticators for cervical cancer patients and C2 ceramide can inhibit tumor cell proliferation in vitro

Autoren

Tilman LR Vogelsang, Verena Kast, Konstantin Bagnjuk, Katja Eubler, Sree Priyanka Jeevanandan, Elisa Schmoeckel, Anna Trebo, Nicole Elisabeth Topalov, Sven Mahner, Doris Mayr, Artur Mayerhofer, Udo Jeschke, Aurelia Vattai

Journal

Frontiers in Oncology 2023 May 1; 13:1110939.

doi: 10.3389/fonc.2023.1110939

Abstract

Introduction: The enzymes Receptor-interacting serine/threonine-protein kinase 1 (RIPK1) und 3 (RIPK3) as well as the protein Mixed lineage kinase domain like pseudokinase (pMLKL) play a role in the signaling cascade of necroptosis. This is a form of programmed cell death which is caspase-independent. High-risk human papilloma virus infection can inhibit necroptosis. Thereby, a persistent infection and consequently the development of cervical cancer can be triggered. Aim of this study was the analysis of the expression of RIPK1, RIPK3 and pMLKL in cervical cancer tissue and the evaluation of its prognostic value on overall survival, progression-free survival and additional clinical parameters.

Methods: The expression of RIPK1, RIPK3, and pMLKL in cervical cancer tissue microarrays of n = 250 patients was analyzed immunohistochemically. Further, the effect of C2 ceramide on several cervical cancer cell lines (CaSki, HeLa, SiHa) was examined. C2 ceramide is a biologically active short-chain ceramide that induces necroptosis in human luteal granulosa cells.

Results: Significantly longer overall survival and progression-free survival rates could be detected in cervical cancer patients expressing nuclear RIPK1 or RIPK3 alone or simultaneously (RIPK1 and RIPK3). Cell viability and proliferation was reduced through C2 ceramide stimulation of cervical cancer cells. Simultaneous stimulation of C2 ceramide and the pan-caspase inhibitor Z-VAD-fmk, or the RIPK1-inhibitor necrostatin-1, partly

reversed the negative effect of C2 ceramide on cell viability. This observation could imply that caspase-dependent and -independent forms of cell death, including necroptosis, can occur. AnnexinV-FITC apoptosis staining induced a significant increase in apoptotic cells in CaSki and SiHa cells. The stimulation of CaSki cells with C2 ceramide led to a significant percentual increase in necrotic/intermediate (dying) cells after stimulation with C2 ceramide. In addition, after stimulation with C2 ceramide, CaSki and HeLa cells live cell imaging showed morphological changes which are common for necroptosis.

Discussion: In conclusion, RIPK1 and RIPK3 are independent positive predictors for overall survival and progression-free survival in cervical cancer patients. C2 ceramide can reduce cell viability and proliferation in cervical cancer cells by inducing most likely both apoptosis and necroptosis.

frontiers | Frontiers in Oncology

TYPE Original Research
PUBLISHED 01 May 2023
DOI 10.3389/fonc.2023.1110939

OPEN ACCESS

EDITED BY
Kari Ring,
University of Virginia, United States

REVIEWED BY
Jixin Dong,
University of Nebraska Medical Center, United States
Ni Zeng,
Affiliated Hospital of Zunyi Medical University, China

*CORRESPONDENCE
Udo Jeschke
udo.jeschke@med.uni-muenchen.de

SPECIALTY SECTION
This article was submitted to Gynecological Oncology, a section of the journal Frontiers in Oncology

RECEIVED 29 November 2022
ACCEPTED 03 April 2023
PUBLISHED 01 May 2023

CITATION
Vogelsang TLR, Kast V, Bagnjuk K, Eubler K, Jeevanandan SP, Schmoeckel E, Trebo A, Topalov NE, Mahner S, Mayr D, Mayerhofer A, Jeschke U and Vattai A (2023) RIPK1 and RIPK3 are positive prognosticators for cervical cancer patients and C2 ceramide can inhibit tumor cell proliferation *in vitro*. *Front. Oncol.* 13:1110939. doi: 10.3389/fonc.2023.1110939

RIPK1 and RIPK3 are positive prognosticators for cervical cancer patients and C2 ceramide can inhibit tumor cell proliferation *in vitro*

Tilman L. R. Vogelsang[1], Verena Kast[2], Konstantin Bagnjuk[2], Katja Eubler[2], Sree Priyanka Jeevanandan[2], Elisa Schmoeckel[3], Anna Trebo[1], Nicole Elisabeth Topalov[1], Sven Mahner[1], Doris Mayr[3], Artur Mayerhofer[2], Udo Jeschke[1,4]* and Aurelia Vattai[1]

[1]Department of Obstetrics and Gynecology, University Hospital, Ludwig-Maximilians-University (LMU) Munich, Munich, Germany, [2]Biomedical Center Munich (BMC), Cell Biology, Anatomy III, Ludwig-Maximilians-University (LMU) Munich, Planegg, Germany, [3]Faculty of Medicine, Institute of Pathology, Ludwig-Maximilians-University (LMU) Munich, Munich, Germany, [4]Department of Obstetrics and Gynecology, University Hospital Augsburg, Augsburg, Germany

Introduction: The enzymes Receptor-interacting serine/threonine-protein kinase 1 (RIPK1) und 3 (RIPK3) as well as the protein Mixed lineage kinase domain like pseudokinase (pMLKL) play a role in the signaling cascade of necroptosis. This is a form of programmed cell death which is caspase-independent. High-risk human papilloma virus infection can inhibit necroptosis. Thereby, a persistent infection and consequently the development of cervical cancer can be triggered. Aim of this study was the analysis of the expression of RIPK1, RIPK3 and pMLKL in cervical cancer tissue and the evaluation of its prognostic value on overall survival, progression-free survival and additional clinical parameters.

Methods: The expression of RIPK1, RIPK3, and pMLKL in cervical cancer tissue microarrays of n = 250 patients was analyzed immunohistochemically. Further, the effect of C2 ceramide on several cervical cancer cell lines (CaSki, HeLa, SiHa) was examined. C2 ceramide is a biologically active short-chain ceramide that induces necroptosis in human luteal granulosa cells.

Results: Significantly longer overall survival and progression-free survival rates could be detected in cervical cancer patients expressing nuclear RIPK1 or RIPK3 alone or simultaneously (RIPK1 and RIPK3). Cell viability and proliferation was reduced through C2 ceramide stimulation of cervical cancer cells. Simultaneous stimulation of C2 ceramide and the pan-caspase inhibitor Z-VAD-fmk, or the RIPK1-inhibitor necrostatin-1, partly reversed the negative effect of C2 ceramide on cell viability. This observation could imply that caspase-dependent and -independent forms of cell death, including necroptosis, can occur. AnnexinV-FITC apoptosis staining induced a

significant increase in apoptotic cells in CaSki and SiHa cells. The stimulation of CaSki cells with C2 ceramide led to a significant percentual increase in necrotic/intermediate (dying) cells after stimulation with C2 ceramide. In addition, after stimulation with C2 ceramide, CaSki and HeLa cells live cell imaging showed morphological changes which are common for necroptosis.

Discussion: In conclusion, RIPK1 and RIPK3 are independent positive predictors for overall survival and progression-free survival in cervical cancer patients. C2 ceramide can reduce cell viability and proliferation in cervical cancer cells by inducing most likely both apoptosis and necroptosis.

KEYWORDS

necroptosis, programmed cell death, cervical cancer, human papillomavirus, RIPK1, RIPK3, pMLKL, C2 ceramide

1 Introduction

Necroptosis is a caspase-independent form of regulated lytic cell death which was first described in 2005 as a contributor to delayed ischemic brain injury *in vivo* (1). Even though it is morphologically similar to necrosis (organelle swelling, plasma membrane rupture, inflammatory response), necroptosis is dependent on a highly regulated signaling cascade (2). Necroptosis might have evolved as a host defense mechanism against intracellular pathogens encoding caspase 8 (casp8) inhibitors (3, 4) but is of high pathophysiological relevance in several medical conditions such as cardiovascular diseases (atherosclerosis (5), myocardial infarction and stroke (6–8), ischemia-reperfusion injury (9)), pancreatitis (10), inflammatory bowel disease and necrotizing enterocolitis (4, 11–13). In cancer, necroptosis is of interest since escape of regulated cell death and inflammation play an important role in tumorigenesis (14).

Cervical cancer is the fourth most common cancer in females worldwide with approximately 604.000 new cases and an estimated 342.000 deaths in 2020 (15). Over the last 30 years the high incidence rate could be reduced due to early diagnosis and effective prevention, screening (i.e. Pap smear test) and treatment programs (16, 17). Persistent infection with high-risk human papilloma virus (hr-HPV) is a key factor for cervical cancer to develop (18). The viral oncoproteins high-risk E6 (hr-E6) and high-risk E7 (hr-E7) disturb the cell cycle, promote hyperproliferation and genomic instability and block apoptosis to promote immortalization (19). Furthermore, hr-HPV suppresses the induction of necroptosis by downregulating the expression of its key regulator receptor-interacting serine/threonine-protein kinase 3 (RIPK3) allowing infected keratinocytes to partially evade the immune system and potentially lead to the progression of hr-HPV induced lesions (20).

Necroptosis is induced *via* activation of Z-DNA binding protein 1 (ZBP1, also known as DAI and DLM-1), tumor necrosis factor receptor 1 (TNFR1), toll-like receptor 3 (TLR3)-TIR domain-containing adaptor protein inducing IFNβ (TRIF), TLR4-TRIF (21) or interferons (22). The necroptotic pathway critically depends on MLKL and RIPK3 (23). After activation, e.g., through binding of ZBP1 to RIPK3 (21), RIPK3 oligomerizes and forms a complex with mixed lineage kinase domain-like protein (MLKL) leading to its phosphorylation (pMLKL) which induces membrane pore induction, disruption of membrane integrity and the release of cell DAMPs (24–26). The role of Receptor-interacting serine/threonine-protein kinase 1 (RIPK1) in necroptosis is more complex, since RIPK1 plays an important role in several pathways. Ligation of TNFR1 can lead to either induction of the NF-κB pathway (gene expression of proinflammatory and prosurvival factors), apoptosis, or necroptosis (27–30). After ligation of TNFR1, RIPK1 among others is recruited and ubiquitinated mediated by cellular inhibitor of apoptosis protein 1 and 2 (cIAP1/2) leading to the induction of the NF-κB pathway (31). When RIPK1 is deubiquitylated by the absence or inhibition of cIAP1/2, RIPK1 is released from TNFR1 and recruits Fas-ligand associated protein with death domain (FADD) which itself recruits procaspase 8 (procasp8) (32). Procasp8 then oligomerizes and autocatalyzes to autoactivate and induce apoptosis (32). When casp8 is inhibited, RIPK3 is activated through autophosphorylation leading to the induction of necroptosis (32).

Abbreviations: Casp8, Caspase 8; hr-HPV, high-risk human papilloma virus; hr-E6/hr-E7, high-risk E6/high-risk E7; RIPK3, receptor-interacting serine/threonine-protein kinase 3; ZBP1, Z-DNA binding protein 1; DAI, DNA dependent activator of interferon regulatory factors (=ZBP1); DLM-1, (=ZBP1); TNFR1, tumor necrosis factor receptor 1; TLR, toll like receptor; TRIF, TIR domain-containing adaptor protein inducing IFNβ; MLKL, mixed lineage kinase domain like protein; pMLKL, phosphorylated MLKL; RIPK1, receptor-interacting serine/threonine-protein kinase 1; cIAP, by cellular inhibitor of apoptosis protein; FADD, Fas-ligand associated protein with death domain; Procasp8, procaspase 8; OS, overall survival; PFS, progression free survival; TMA, tissue micro array; FFPE, formalin fixed paraffin embedded; PBS, phosphate buffer saline; TBS, Tris buffered saline; IRS, immunoreactive score; MTT, Thiazolyl Blue Tetrazolium Bromide; DMSO, dimethyl sulfoxide; BrdU, bromodeoxyuridine; Nec-1, necrostatin-1; pRb, retinoblastoma protein; FLIP, FLICE-like inhibitory protein; NRF, necrosis-related factor.

Ceramide is a central molecule in sphingolipid metabolism which can function as a tumor suppressor lipid (33), inducing apoptotic responses in neuroblastoma cells (34) and breast cancer cells (35). In human luteal granulosa cells necroptosis can be induced through stimulation with the soluble C2 ceramide (36).

Aim of this study was to analyze the expression of RIPK1, RIPK3, and pMLKL in cervical carcinoma patient tissue and to correlate their expression with clinical parameters, overall survival (OS) and progression-free survival (PFS). Another goal was the stimulation of cervical carcinoma cell lines CaSki, HeLa, and SiHa with C2 ceramide and to characterize its impact on induction of necroptosis or apoptosis, cell viability and cell proliferation.

2 Materials and methods

2.1 Characteristics of patients and biopsies

All assessable cervical cancer patients (n = 250) who had undergone surgery for treatment of cervical cancer at the Department of Gynecology and Obstetrics, Ludwig-Maximilians-University Munich, Germany, from 1993 until 2002 and whose paraffin-embedded tumor tissue was available were included in this study. Patients were not pre-selected. An experienced gynecological pathologist assigned histopathological tumor subtypes (squamous cell carcinoma, adenocarcinoma, adenosquamous carcinoma) and grading (G1: well differentiated, G2: moderately differentiated, G3: poorly differentiated). TNM classification (T = primary tumor site, N = regional lymph node involvement, M = presence of distant metastatic spread) was carried out as published by the Union for International Cancer Control (UICC). FIGO classification was evaluated according to the criteria of the Fédération Internationale de Gynécologie et d'Obstétrique (FIGO). Clinical and patient follow-up data was received from the Munich Cancer Registry (Table 1). The mean age of patients at diagnosis was 49.0 ± 13.0 years with a range between 20.4 and 83.3 years. Patients who died independently of their tumor or whose cause of death is unknown were censured. Other histopathological parameters were examined and published previously, enabling correlation analysis to the parameters investigated in this study.

2.2 Immunohistochemistry

Directly after surgical resection, the samples were fixed in neutral-buffered formalin (3.7%) followed by standardized paraffin embedding. Tissue micro arrays (TMAs) were then prepared from formalin fixed paraffin embedded (FFPE) cervical

TABLE 1 Description of clinical and pathological variables of the patients.

	number of cases (total number of cases: n=250)	%
histopathological tumor subtype		
squamous cell carcinoma	194	77.6
adenocarcinoma	34	13.6
adenosquamous carcinoma	15	6.0
unknown	7	2.8
tumor grading		
G1	21	8.4
G2	143	57.2
G3	78	31.2
unknown	8	3.2
extent of primary tumor (pT)		
pT1	107	42.8
pT2	126	50.4
pT3	9	3.6
pT4	1	0.4
unknown	7	2.8
regional lymph node involvement (pN)		
pN0	145	58.0
pN1	98	39.2

(Continued)

TABLE 1 Continued

	number of cases (total number of cases: *n*=250)	%
unknown	7	2.8
presence of distant metastatic spread (pM)		
pM0	2	0.8
pM1	7	2.8
pMX	235	94
unknown	6	2.4
FIGO classification		
FIGO I	79	31.6
FIGO II	64	25.6
FIGO III	93	37.2
FIGO IV	7	2.8
unknown	7	2.8
progression		
none	180	72.0
at least one	63	25.2
unknown	7	2.8
survival		
censured	211	84.4
dead (tumor-dependent)	33	13.2
unknown	6	2.4

cancer samples. The tissue sections (3µm) were dewaxed in Roticlear (Carl Roth GmbH + Co. KG, Karlsruhe, Germany) for 20 min followed by immersion in 3% H_2O_2 in methanol at room temperature (RT) for 20 min to inactivate endogenous peroxidase. A descending ethanol gradient (S99%, 70% and 50%) was used to rehydrate the specimens. The sections were prepared for epitope retrieval in a pressure cooker for 5 min using sodium citrate buffer (pH 6.0; 0.1 mol/L citric acid/0.1 mol/L sodium citrate) followed by washing in distilled water and phosphate buffer saline (PBS) (RIPK1 and RIPK3 staining) or Tris buffered saline (TBS) (pMLKL staining). To block non-specific binding of primary antibodies, Blocking Solution (reagent 1, ZytoChem Plus HRP Polymer System (Mouse/Rabbit); Zytomed Systems GmbH, Berlin, Germany) was applied for 5min at RT for RIPK1 and RIPK3 staining. For pMLKL staining, non-specific binding of primary antibodies was blocked by applying blocking serum (= two drops of normal goat serum diluted in 10ml sterile TBS; VECTASTAIN Elite ABC-HRP Kit, Peroxidase (Rabbit IgG) – PK6101; Vector Laboratories, Inc., Burlingame, CA, USA) for 20 min at RT. Specimens were then separately incubated with the following primary antibodies: anti-RIPK1 (polyclonal rabbit IgG, HPA015257; Sigma Aldrich, St. Louis, MO, USA) for 17h at 4°C followed by 30min at RT in a 1:50 dilution in PBS, anti-RIPK3 (polyclonal rabbit IgG;, HPA055087 Sigma Aldrich, St. Louis, MO, USA) for 16h at 4°C in a 1:1500 dilution in PBS and anti-MLKL (phospho S358) (monoclonal Rabbit IgG, ab187091; Abcam, Cambridge, UK) for 16h at 4°C in a 1:100 dilution in TBS. Then, the tissue slides for RIPK1 and RIPK3 staining were incubated with PostBlock Reagent (reagent 2) for 20 min and HRP-Polymer (Mouse/Rabbit) (reagent 3) for 30 min which contain secondary antibodies (anti-mouse/-rabbit) and peroxidase according to the manufacturer's protocol (reagent 2, reagent 3, ZytoChem Plus HRP Polymer System (Mouse/Rabbit); Zytomed Systems GmbH, Berlin, Germany). The tissue slides for pMLKL staining were incubated with the secondary antibody (= two drops of normal goat serum and one drop of biotinylated goat anti-rabbit IgG diluted in 10ml sterile TBS; VECTASTAIN Elite ABC-HRP Kit, Peroxidase (Rabbit IgG) – PK6101) for 30 min followed by incubation with ABC complex (= four drops of Reagent A and four drops of Reagent B diluted in 10ml sterile TBS; VECTASTAIN Elite ABC-HRP Kit, Peroxidase (Rabbit IgG) – PK6101) for 30 min. All slides were washed with PBS (RIPK1, RIPK3) or TBS (pMLKL) after every incubation step. Next, 3,3′-diaminobenzidine chromogen (DAB; Dako, Glostrup, Denmark) and the according substrate buffer (Liquid DAB and Substrate Chromogen System, DAKO, Munich, Germany) were added to the slides. The slides were washed in distilled water to stop the reaction followed by counterstaining in Mayer's acidic hematoxylin. The slides were then immersed in an

ascending ethanol gradient and Roticlear and finally cover slipped using ROTI® Mount (Carl Roth GmbH + Co. KG, Karlsruhe, Germany). Appropriate tissue was used as positive control (placenta for RIPK1, RIPK3 and pMLKL) and negative controls (placenta for RIPK1 and pMLKL and colon for RIPK3) (Figure S2). For the negative controls the primary antibodies were each replaced with a specific isotype control antibody (BioGenex, Fremont, CA, USA).

2.3 Quantification

The immunohistochemically stained cervical cancer specimens were examined using a Leitz Diaplan photomicroscope (Leitz, Wetzlar, Germany). Quantification of RIPK1, RIPK3, and pMLKL expression was performed by applying the semiquantitative immunoreactive score (IRS) which evaluates the intensity and distribution pattern of antigen expression (37). The IRS is calculated by multiplying the number of positively stained cells (in %) (0: no staining; 1: 1% - 10% stained tumor cells; 2: 11% - 50% stained tumor cells; 3: 51% - 80% stained tumor cells; 4: > 80% stained tumor cells) with the predominant staining intensity (0: none; 1: weak; 2: moderate; 3: strong). The scale goes from 0 (no expression) to 12 (very high expression). Images were taken with Flexacam C1 (Leica Microsystems (Switzerland) Ltd., Heerbrugg, Switzerland).

2.4 Cell lines

The human cervical cancer cell lines CaSki (epidermoid carcinoma), HeLa (adenocarcinoma) and SiHa (squamous cell carcinoma) obtained from ATCC (Rockville, MD, USA) were used for *in vitro* studies. They were maintained in culture using RPMI Medium 1640 (1X) + GlutaMAX (ThermoFisher Scientific, Waltham, MA, USA) supplemented with 10% fetal bovine serum at standard conditions (humidified incubator at 37°C and 5% CO_2 saturation).

2.5 MTT assay

Cell viability was analyzed using Thiazolyl Blue Tetrazolium Bromide (MTT; Sigma Aldrich, St. Louis, MO, USA; M5655). After 24h, 48h, and 72h of stimulation incubation, 20µl of Thiazolyl Blue Tetrazolium Bromide (5mg MTT/ml sterile PBS) was added to each well followed by soft shaking on a plate shaker for 5 min and incubation for 1.5h at 37°C in a 5% CO_2 humidified atmosphere. Then, the supernatant was removed and 200µl dimethyl sulfoxide (DMSO)/well was added to solubilize the blue crystals. After 5 min of soft shaking on a plate shaker, optical density was evaluated at wavelengths of 595nm by the Elx800 universal microplate reader (BioTek Instruments GmbH, Bad Friedrichshall, Germany) and Gen5 software (BioTek Instruments GmbH, Bad Friedrichshall, Germany). All tests were repeated three times with 5 wells per concentration.

2.6 BrdU assay

For analysis of cell proliferation, the colorimetric bromodeoxyuridine (BrdU) assay was performed using the Cell Proliferation ELISA, BrdU (colorimetric) kit from Roche (F. Hoffmann-La Roche AG, Basel, Switzerland). The assay was performed according to the manufacturer's protocol. CaSki, HeLa and SiHa cells were incubated with C2 ceramide for 24h, 48h and 72h in 96-well plates as described below. Then, BrdU was added, and the cells were incubated for another 24h. The medium was removed and 200µl FixDenat per well was added to fix the cells and denature the DNA for improvement of accessibility of the incorporated BrdU for detection by the antibody. Next, anti-BrdU-POD was added and bound to the BrdU incorporated in newly synthesized DNA followed by incubation for 90 min at RT. The supernatant was removed, and the wells were washed three times with a washing solution. 100µl substrate solution (tetramethyl-benzidine, TMB) per well was added and incubated in the dark at RT to detect the immune complexes. Visualization of the substrate reaction was an increasing deep blue coloration. After 15 min of incubation, the reaction was stopped by adding sulfuric acid. The plate was then measured at a wavelength of 450nm using the Elx800 universal microplate reader using Gen5 software. All tests were repeated three times and with 5 wells per concentration.

2.7 Stimulation with C2 ceramide

For MTT- and BrdU assay, $5x10^3$ CaSki, HeLa and SiHa cells were incubated in 100µl RPMI Medium 1640 (1X) + GlutaMAX (ThermoFisher Scientific, Waltham, MA, USA) supplemented with 10% FBS in 96-well plates (flat bottom) for four hours. Then, medium with 10% FBS was removed and 100µl medium without FBS was added followed by 24h of incubation.

Stimulation with 50µM, 100µM or 200µM C2 ceramide (Enzo Life Sciences (ELS) AG, Lausen, Switzerland; BML-SL100, Prod.Nr.: ALX-306-024) was performed by dissolving the substance to 200mM (68.3mg/ml) in DMSO followed by dilution of the ceramide/DMSO stock 200-fold into a BSA solution which was prepared using fatty acid-free BSA diluted in water to 66mg/ml (1mM). At first, a precipitate was formed but dissolved after 30-60 min of stirring at RT. Then, the ceramide/DMSO/BSA solution was diluted in 100µl medium without FBS at respective concentrations (100µM, 200µM or 400µM) and added to the wells. The 1:1 dilution in the well gave the final concentration of 50µM, 100µM or 200µM.

Necrostatin-1 (nec-1, Santa Cruz Biotechnology, Inc., Heidelberg, Germany; CAS 4311-88-0) and Z-VAD-fmk (Selleck Chemicals, Munich, Germany; Catalog No. S7023, CAS 187389-52-2) were both dissolved to 50mM and further to 5mM in DMSO. Co-stimulation of C2 ceramide and nec-1 or C2 ceramide and Z-VAD-fmk was initiated by pre-stimulation with 1µM, 5µM, 20µM or 50µM nec-1 or 1µM, 5µM, 20µM or 50µM Z-VAD-fmk for 2h by diluting the substances in 100µl medium without FBS at respective concentrations (2µM, 10µM, 40µM or 100µM) and adding it to the

wells. The 1:1 dilution in the well gave the final concentration of 1µM, 5µM, 20µM or 50µM. Then, the supernatant was removed and co-stimulation of 100µM C2 ceramide and 1µM, 5µM, 20µM or 50µM nec-1 or 100µM C2 ceramide and 1µM, 5µM, 20µM or 50µM Z-VAD-fmk was performed by diluting the substances in 200µl medium without FBS at respective concentrations (100µM C2 ceramide and 1µM, 5µM, 20µM or 50µM nec-1/Z-VAD-fmk) and adding it to the wells. The concentrations of the substances were based on previous studies (36, 38, 39). Unstimulated cells and wells without any cells served as negative controls. A solvent control (DMSO) was always conducted.

2.8 Live-cell imaging

For visualization of C2 ceramide's effect on cervical carcinoma cells, live-cell imaging was performed. Therefore, 5 x10^4 CaSki, HeLa, and SiHa cells were seeded in a glass-bottomed culture dish (µ-Dish, Ø 35 mm; ibidi, Gräfelfing, Germany) and incubated under standard conditions at 37°C and 5% CO_2. The cells were then serum starved for 6h before being stimulated with C2 ceramide by dissolving C2 ceramide as described above. 100 µM of C2 ceramide diluted in medium without FBS was added to the cells, and cells were imaged for 72 h using an Axiovert 135 microscope (Carl Zeiss). To produce a time-lapse series (Micro-Manager 1.3 Microscopy Software Ron Vale's laboratory at UCSF, USA), images (ProgRes MF, Jenoptik, Jena, Germany) were taken every 20 minutes. iMovie 9.0.3 (Apple Inc., Cupertino, CA, USA) was used to create movie sequences.

2.9 Western blot

Cells were cultured under basal conditions and harvested. The method was described before (36). In brief, cellular protein was isolated using RIPA buffer containing protease and phosphatase inhibitors (PI, Thermo Fisher Scientific, Waltham, USA) and 16 µg were loaded onto a SDS-PAGE gel. Primary antibody (anti-RIPK3, polyclonal rabbit IgG, HPA055087, Lot: R73206, Sigma Aldrich, St. Louis, MO, USA) and secondary antibody (IRDye® 680RD Donkey anti-Rabbit IgG, Secondary Antibody) were used.

2.10 Cell death detection by flow cytometry

For quantitative detection of cell death, Annexin V-FITC (ALX-209-256-T100, Enzo Life Sciences, Farmingdale, NY, USA) and SYTOX™ Red Dead Cell Stain (S34859, Invitrogen, Carlsbad, CA, USA) based flow cytometry was performed. Briefly, 2 x 10^5 CaSki, HeLa, or SiHa cells were seeded and after a 6h starvation step on medium without FBS the next day cells were treated with 100µM C2 ceramide or the solvent control for 72h, as described above. Cells were trypsinized, washed in PBS and resuspended in a buffer consisting of 10mM HEPES, 140mM NaCl and 2.5mM $CaCl_2$ at pH 7.4, followed by incubation with Annexin V-FITC for 10 minutes according to the manufacturer's instructions, and addition of SYTOX Red Dead Cell Stain (1:1000). Labelled cells were sorted using the BD FACSCanto™ II (Becton, Dickinson and Company, Franklin Lakes, NJ, USA) and signals (Annexin V-FITC: 488nm, 530/30 bandpass filter; SYTOX™ Red Dead Cell Stain: 633nm excitation, 660/20 bandpass filter) were analyzed with the BD FACSDiva Software (version 8.0.1, Becton, Dickinson and Company). This was repeated two times (n = 2).

2.11 Statistical analysis

For statistical analysis, IBM SPSS Statistics Version 26.0.0.0 (IBM, Armonk, New York, NY, USA) was used. p-values of $p < 0.05$ were considered statistically significant. Kruskal-Wallis-H test was applied as appropriate for group comparisons of independent groups regarding clinical and pathological subgroups. Bivariate correlations between staining results in this study and other variables and clinicopathological data were determined using Spearman's rank correlation coefficient. Differences in OS and PFS times of cervical cancer patients were tested for significance by log-rank (Mantel-Cox) test and visualized using Kaplan-Meier curves. Cox regression analysis was used to ascertain the independence of the investigated prognosticators. Variables included in the Cox regression model were patient's age, histological subtype, tumor grading, FIGO, nodal status, RIPK1, RIPK3, co-expression of RIPK1 and RIPK3, and co-expression of RIPK1, RIPK3, and pMLKL. RIPK1, RIPK3, and pMLKL expression were divided into low and high expression for survival analysis. All *in vitro* analyses were statistically analyzed using Wilcoxon test and visualized with GraphPad Prism 7.00 (San Diego, CA, USA). For statistical analysis of AnnexinV-FITC apoptosis staining followed by FACS analysis the percentual number of apoptotic cells after treatment was compared to the percentual number of apoptotic cells in the control and the percentual number of necrotic and intermediate (dying) cells after treatment was compared to the percentual number of necrotic and intermediate (dying) cells in the control using Wilcoxon test.

2.12 Ethical approval and informed consent

The study was approved by the local ethics committee of Ludwig-Maximilians University of Munich, Germany (approval number 259-16, 2016). All tissue samples examined in this study were obtained from material from the archives of the Department of Gynecology and Obstetrics, Ludwig-Maximilians University of Munich. The material used in this study was fully anonymized, declared as left over after finalizing all diagnostic procedures and was used more than 10 years after surgery. All experiments involving human participants were performed according to the standards of the Declaration of Helsinki from 1964 and its later amendments and were in accordance with the ethical standards of the institutional and/or national research committee. During analyses, the observers were fully blinded for patients' data.

3 Results

3.1 Expression of RIPK1, RIPK3, and pMLKL in cervical cancer and correlation with various clinical and pathological parameters

Immunohistochemical staining showed that RIPK1 and pMLKL were expressed in the nucleus and cytoplasm while RIPK3 was expressed in the nucleus in cervical cancer tissue. Differences in expression of RIPK1, RIPK3, and pMLKL were examined by comparing the immunoreactive score (IRS) in the groups of histological subtypes (squamous cell carcinoma, adenocarcinoma, adenosquamous carcinoma), grading (G1-G3), TNM- and FIGO-classification.

3.1.1 Correlation of RIPK1, RIPK3, and pMLKL with grading and histology

Nuclear RIPK3 expression was significantly higher in cervical cancer tissue with low grading (G1) compared to grading G2 and G3 ($p = 0.011$) (Figures 1A–D).

Nuclear pMLKL expression correlated significantly with low grading (G1) in comparison to grading G2 and G3 ($p = 0.010$) (Figures 1E–H). In grading G1, cytoplasmic pMLKL was expressed significantly higher compared to grading G2 and G3 ($p < 0.001$) (Figures 1I–L).

A comparison of grading with nuclear and cytoplasmic RIPK1 using Kruskal-Wallis test showed no significant correlation.

Differences in nuclear pMLKL expression regarding histological subtypes (squamous cell carcinoma, adenocarcinoma, adenosquamous carcinoma) were significant ($p = 0.033$) with

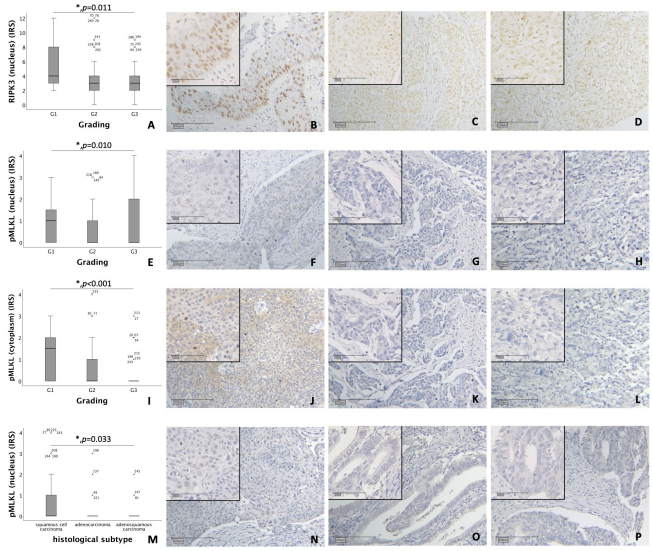

FIGURE 1
(A–D) Correlation of nuclear RIPK3 expression with tumor grading in cervical carcinoma (p = 0.011). **(A)** boxplot of nuclear RIPK3 expression and tumor grading in cervical carcinoma. **(B)** cervical carcinoma, grading G1 (n = 18) with a nuclear RIPK3 IRS of 6, magnification x10 and x25 in the inset. **(C)** cervical carcinoma, grading G2 (n = 131) with a nuclear RIPK3 IRS of 3, magnification x10 and x25 in the inset. **(D)** cervical carcinoma, grading G3 (n = 74) with a nuclear RIPK3 IRS of 3, magnification x10 and x25 in the inset. **(E–H)** Correlation of nuclear pMLKL expression with tumor grading in cervical carcinoma (p = 0.010). **(E)** boxplot of nuclear pMLKL expression and tumor grading in cervical carcinoma. **(F)** cervical carcinoma, grading G1 (n = 16) with a nuclear pMLKL IRS of 3, magnification x10 and x25 in the inset. **(G)** cervical carcinoma, grading G2 (n = 119) with a nuclear pMLKL IRS of 0, magnification x10 and x25 in the inset. **(H)** cervical carcinoma, grading G3 (n = 72) with a nuclear pMLKL IRS of 0, magnification x10 and x25 in the inset. **(I–L)** Correlation of cytoplasmic pMLKL expression with tumor grading in cervical carcinoma (p < 0.001). **(I)** boxplot of cytoplasmic pMLKL expression and tumor grading in cervical carcinoma. **(J)** cervical carcinoma, grading G1 (n = 16) with a cytoplasmic pMLKL IRS of 3, magnification x10 and x25 in the inset. **(K)** cervical carcinoma, grading G2 (n = 119) with a cytoplasmic pMLKL IRS of 0, magnification x10 and x25 in the inset. **(L)** cervical carcinoma, grading G3 (n = 72) with a cytoplasmic pMLKL IRS of 0, magnification x10 and x25 in the inset. **(M–P)** Correlation of nuclear pMLKL expression with histological subtype in cervical carcinoma (p = 0.033). **(M)** boxplot of nuclear pMLKL expression and histological subtype in cervical carcinoma. **(N)** cervical squamous cell carcinoma (n = 169) with a nuclear pMLKL IRS of 2, magnification x10 and x25 in the inset. **(O)** cervical adenocarcinoma (n = 23) with a nuclear pMLKL IRS of 0, magnification x10 and x25 in the inset. **(P)** cervical adenosquamous carcinoma (n = 13) with a nuclear pMLKL IRS of 0, magnification x10 and x25 in the inset.

similar medians (IRS = 0) (Figures 1M–P). No significant correlation was found when comparing histological subtype with nuclear or cytoplasmic RIPK1 expression, nuclear RIPK3 expression or cytoplasmic pMLKL expression.

3.1.2 Correlation of RIPK1, RIPK3, and pMLKL with TNM- and FIGO-classification

Nuclear RIPK3 overexpression significantly correlated with low pT (pT1) with a median IRS of 4 in comparison to pT2, pT3 and pT4 with a median IRS of 3 (p = 0.004) (Figure 2A). Increasing grade of FIGO was associated with decreasing expression of RIPK3 in the nucleus (p = 0.022) (Figure 2B). Differences in the expression of nuclear RIPK3 regarding regional lymph node involvement (pN) were significant (p = 0.016) with similar medians (IRS = 3) (Figure 2C). Expression of cytoplasmic pMLKL correlated with pN showed significant (p = 0.030) differences with similar medians (IRS = 0) (Figure 2D). A small subgroup of patients diagnosed with cervical carcinoma FIGO IV (n = 7) had a significantly (p = 0.033) higher nuclear pMLKL expression (IRS = 3) (Figure 2E).

The correlation between nuclear and cytoplasmic RIPK1 expression and TNM- and FIGO classification showed no significance.

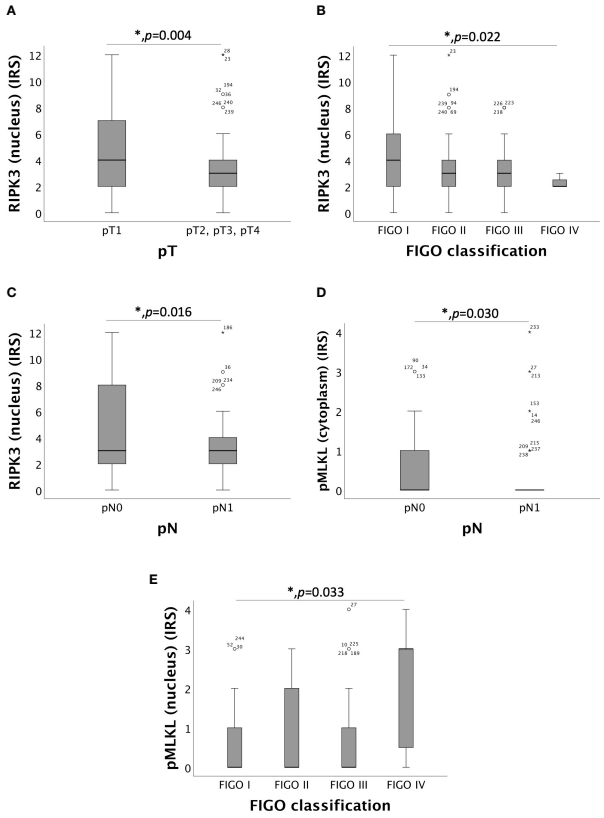

FIGURE 2
Correlation of RIPK3 and pMLKL with pT, pN and FIGO-classification. **(A)** boxplot of nuclear RIPK3 expression and the size or the extent of the primary tumor (pT) in cervical carcinoma (p = 0.004), median IRS of nuclear RIPK3 in pT1 was 4 (n = 96) and in pT2, pT3 and pT4 was 3 (n = 130). **(B)** boxplot of nuclear RIPK3 expression and FIGO classification in cervical carcinoma (p = 0.022), median IRS of nuclear RIPK3 in FIGO I was 4 (n = 69), in FIGO II was 3 (n = 61), in FIGO III was 3 (n = 89) and in FIGO IV was 2 (n = 7). **(C)** boxplot of nuclear RIPK3 expression and regional lymph node status (pN) in cervical carcinoma (p = 0.016), median IRS of nuclear RIPK3 expression in pN0 was 3 (n = 133) and in pN1 was 3 (n = 93). **(D)** boxplot of cytoplasmic pMLKL expression and regional lymph node status (pN) in cervical carcinoma (p = 0.030), median IRS of cytoplasmic pMLKL expression in pN0 was 0 (n = 120) and in pN1 was 0 (n = 87). **(E)** boxplot of nuclear pMLKL expression and FIGO classification in cervical carcinoma (p = 0.033), median IRS of nuclear pMLKL in FIGO I was 0 (n = 61), in FIGO II was 0 (n = 58), in FIGO III was 0 (n = 81) and in FIGO IV was 3 (n = 7).

3.1.3 Correlation of RIPK1, RIPK3, and pMLKL with histopathological parameters

Spearman's rank correlation coefficient was evaluated for RIPK1, RIPK3, pMLKL and various histopathological markers which were stained and analyzed in the applied cervical cancer patient collective of previous studies (Tables S1, S2, S3). RIPK1, RIPK3, and pMLKL showed significant correlations with each other. Nuclear RIPK1 significantly correlated with cytoplasmic RIPK1 (Spearman rho: 0.486, $p < 0.001$), nuclear RIPK3 (Spearman rho: 0.414, $p < 0.001$), nuclear pMLKL (Spearman rho: 0.184, $p = 0.009$) and cytoplasmic pMLKL (Spearman rho: 0.310, $p < 0.001$). Cytoplasmic RIPK1 significantly correlated with RIPK3 (Spearman rho: 0.471, $p < 0.001$), nuclear pMLKL (Spearman rho: 0.168, $p = 0.016$) and cytoplasmic pMLKL (Spearman rho: 0.278, $p < 0.001$). Nuclear RIPK3 correlated significantly with nuclear pMLKL (Spearman rho: 0.158, $p = 0.025$) and cytoplasmic pMLKL (Spearman rho: 0.271, $p < 0.001$). Nuclear pMLKL correlated significantly with cytoplasmic pMLKL (Spearman rho: 0.363, $p < 0.001$).

In cervical cancer tissue, nuclear p53 not only correlated significantly with nuclear RIPK1 (Spearman rho: 0.274, $p < 0.001$), cytoplasmic RIPK1 (Spearman rho: 0.318, $p < 0.001$) and nuclear RIPK3 (Spearman rho: 0.205, $p = 0.002$) but also with cytoplasmic pMLKL (Spearman rho: 0.171, $p = 0.014$).

hr-HPV protein E7 not only interferes with pRb (retinoblastoma protein) but also with p21, an important regulator of the cell cycle (40). In our study, p21 correlated significantly with proteins relevant for necroptosis: p21 showed a positive correlation with nuclear RIPK1 (Spearman rho: 0.217, $p = 0.003$), cytoplasmic RIPK1 (Spearman rho: 0.311, $p < 0.001$), nuclear RIPK3 (Spearman rho: 0.154, $p = 0.039$) and nuclear pMLKL (Spearman rho: 0.197, $p = 0.012$).

E6 is an important human papilloma virus oncoprotein as one of its key functions is degradation of p53 (18). E6 correlated negatively with nuclear (Spearman rho: *-0.151*, $p = 0.030$) and cytoplasmic (Spearman rho: *-0.157*, $p = 0.025$) pMLKL.

3.2 Correlation of RIPK1, RIPK3, and pMLKL with OS and PFS in cervical cancer patients

3.2.1 Nuclear RIPK1 expression correlated with longer OS and PFS in cervical cancer patients

Nuclear RIPK1 expression (IRS > 0) was associated with increased survival. Patients expressing RIPK1 in the nucleus had a significantly longer OS ($p = 0.029$) and PFS ($p = 0.013$) (Figures 3A, B). Multivariate Cox regression analysis was conducted to test for independent prognosticators for OS and PFS in the cohort of $n = 250$ cervical cancer patients and significantly showed that nuclear RIPK1 expression is an independent prognosticator for OS (Table 2) and PFS (Table 3).

To validate the overall survival and progression-free survival of the RIPK1 gene in a large independent cervical squamous cell carcinoma cohort, the *KM plotter* database was used (41). Sources of the *KM plotter* database include GEO, EGA and TCGA (41). Specifically, the use of GEO and TCGA datasets have already been published on cervical cancer (42, 43). We divided patients into high and low groups of expression of RIPK1 using auto select best cut-off. OS was the chosen to compare these groups. A follow-up threshold of 60 months was chosen. The results showed that the overall survival time of patients in the high-RIPK1 expression group ($n = 189$) was significantly longer than that of the low-expression group ($n = 115$) ($p = 0.04$) (Figure S3). The progression-free survival of patients in the high-RIPK1 expression group ($n = 131$) was insignificantly worse compared to patients in the low-expression group ($n = 43$). This correlates with the results of our cohort even though we did not use the C-index, which is a useful tool for analysing different datasets (42, 43).

3.2.2 High nuclear RIPK3 expression correlated with longer OS and PFS in cervical cancer patients

High nuclear RIPK3 expression (IRS > 3) was correlated significantly with a longer OS ($p = 0.010$) as well as a longer PFS ($p = 0.004$) (Figures 3C, D). To test for independent prognosticators for OS and PFS in the cohort of $n = 250$ cervical cancer patients multivariate Cox regression analysis was performed. It significantly showed that nuclear RIPK3 expression was an independent prognosticator for PFS (Table 4) but not for OS (Table 5).

3.2.3 Co-expression of nuclear RIPK1 and RIPK3 correlated with longer OS and PFS in cervical cancer patients

Patients expressing both RIPK1 and RIPK3 in the nucleus (IRS > 0) had a significantly longer OS compared to patients only expressing one or none of these markers ($p = 0.028$). Patients expressing either RIPK1 or RIPK3 had a longer OS than patients without any expression (Figure 3E).

Co-expression of RIPK1 and RIPK3 in the nucleus correlated significantly with a longer PFS compared to the expression of only one or none of these two parameters ($p = 0.032$) (Figure 3F). Multivariate Cox regression analysis was conducted to test for independent prognosticators for OS and PFS in the cohort of $n = 250$ cervical cancer patients and significantly showed nuclear co-expression of RIPK1 and RIPK3 as independent prognosticators for OS (Table 6) and PFS (Table 7).

3.2.4 Co-expression of RIPK1 and RIPK3 and pMLKL is a positive prognosticator for OS in cervical cancer patients

Patients expressing RIPK1, RIPK3, and pMLKL in the nucleus (IRS > 0) had a significantly longer OS compared to patients only expressing two, one or none of these factors ($p = 0.020$) (Figure 4A). The more factors a cervical cancer patient of this cohort expressed, the longer the OS.

Co-expression of RIPK1 and RIPK3 in the nucleus and cytoplasmic pMLKL (IRS > 0) also correlated with a longer OS compared to patients only expressing two, one or none of these factors ($p = 0.041$) (Figure 4B).

We performed multivariate Cox regression analysis to test for independent prognosticators for OS and PFS in the cohort of $n = 250$ cervical cancer patients. It significantly showed nuclear co-expression of RIPK1, RIPK3, and pMLKL as an independent prognosticator for OS (Table 8). In another multivariate Cox regression analysis, co-expression of nuclear RIPK1, nuclear RIPK3 and cytoplasmic pMLKL presented as a significant independent prognosticator for OS in cervical cancer patients (Table 9).

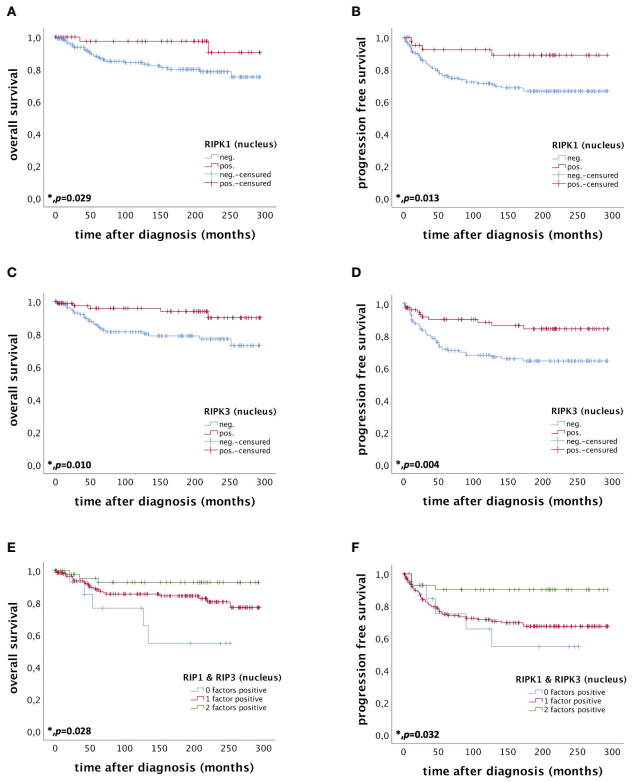

FIGURE 3
OS and PFS of patients diagnosed with cervical cancer correlated with nuclear RIPK1 expression **(A, B)** nuclear RIPK3 expression **(C, D)** and simultaneous expression of RIPK1 and RIPK3 in the nucleus **(E, F)**. **(A)** OS of patients diagnosed with cervical cancer correlated with nuclear RIPK1 expression. Nuclear RIPK1 expression (n = 47) was associated with longer OS in cervical cancer patients compared to patients not expressing RIPK1 (n = 180) (p = 0.029). **(B)** PFS of patients diagnosed with cervical cancer correlated with nuclear RIPK1 expression. Nuclear RIPK1 expression (n = 43) was associated with longer PFS in cervical cancer patients compared to patients not expressing RIPK1 (n = 172) (p = 0.013). **(C)** OS of patients diagnosed with cervical cancer correlated with nuclear RIPK3 expression. High nuclear RIPK3 expression (n = 86) was associated with longer OS in cervical cancer patients compared to patients with low RIPK3 expression (n = 141) (p = 0.010). **(D)** PFS of patients diagnosed with cervical cancer correlated with nuclear RIPK3 expression. High nuclear RIPK3 expression (n = 81) was associated with longer PFS in cervical cancer patients compared to patients with low RIPK3 expression (n = 134) (p = 0.004). **(E)** OS of patients diagnosed with cervical cancer correlated with simultaneous expression of nuclear RIPK1 and RIPK3. Expression of both RIPK1 and RIPK3 (n = 48) in the nucleus was associated with longer OS in cervical cancer patients (p = 0.028) compared to patients expressing only one (n = 162) or no factor (n = 15). **(F)** PFS of patients diagnosed with cervical cancer correlated with simultaneous expression of nuclear RIPK1 and RIPK3. Expression of both RIPK1 and RIPK3 (n = 44) in the nucleus was associated with longer OS in cervical cancer patients (p = 0.032) compared to patients expressing only one (n = 155) or no factor (n = 14).

TABLE 2 Multivariate Cox regression analysis of cervical cancer patients (n = 250) and their clinical and pathological characteristics including nuclear RIPK1 expression regarding OS.

covariate	hazard ratio	95% CI	p-value
patient's age (< 49 yrs vs. ≥ 49 yrs)	2.490	1.173-5.289	0.018*
histological subtype	1.923	1.230-3.005	0.004*
tumor grading	0.977	0.873-1.093	0.683
FIGO	1.022	1.001-1.044	0.040*
nodal status (pNX/0 vs. pN1)	1.514	0.729-3.141	0.266
positive nuclear RIPK1 expression	0.212	0.050-0.893	0.035*

Significant independent factors for OS are indicated with asterisks. (*p < 0.05).

TABLE 3 Multivariate Cox regression analysis of cervical cancer patients (n = 250) and their clinical and pathological characteristics including nuclear RIPK1 expression regarding PFS.

covariate	hazard ratio	95% CI	p-value
patient's age (< 49 yrs vs. ≥ 49 yrs)	1.418	0.810-2.483	0.222
histological subtype	1.647	1.130-2.401	0.009*
tumor grading	0.983	0.902-1.070	0.690
FIGO	1.048	1.024-1.072	< 0.001**
nodal status (pNX/0 vs. pN1)	1.854	1.061-3.240	0.030*
positive nuclear RIPK1 expression	0.304	0.109-0.849	0.023*

Significant independent factors for PFS are indicated with asterisks. (*p < 0.05).

TABLE 4 Multivariate Cox regression analysis of cervical cancer patients (n = 250) and their clinical and pathological characteristics including nuclear RIPK3 expression regarding PFS.

covariate	hazard ratio	95% CI	p-value
patient's age (< 49 yrs vs. ≥ 49 yrs)	1.154	0.654-2.036	0.622
histological subtype	1.408	0.968-2.047	0.073
tumor grading	0.977	0.903-1.057	0.561
FIGO	1.046	1.022-1.070	< 0.001**
nodal status (pNX/0 vs. pN1)	1.966	1.121-3.449	0.018*
positive nuclear RIPK3 expression	0.466	0.288-0.950	0.036*

Significant independent factors for PFS are indicated with asterisks. (*p < 0.05, **p < 0.001).

TABLE 5 Multivariate Cox regression analysis of cervical cancer patients (n = 250) and their clinical and pathological characteristics including nuclear RIPK3 expression regarding OS.

covariate	hazard ratio	95% CI	p-value
patient's age (< 49 yrs vs. ≥ 49 yrs)	1.955	0.915-4.180	0.084
histological subtype	1.596	1.018-2.504	0.042*
tumor grading	0.976	0.885-1.076	0.626
FIGO	1.021	0.999-1.043	0.061
nodal status (pNX/0 vs. pN1)	1.651	0.795-3.427	0.179
positive nuclear RIPK3 expression	0.393	0.147-1.050	0.063

Significant independent factors for OS are indicated with asterisks. (*p < 0.05).

TABLE 6 Multivariate Cox regression analysis of cervical cancer patients (n = 250) and their clinical and pathological characteristics including nuclear RIPK1-RIPK3 co-expression regarding OS.

covariate	hazard ratio	95% CI	p-value
patient's age (< 49 yrs vs. ≥ 49 yrs)	2.336	1.098-4.967	0.028*
histological subtype	1.722	1.101-2.692	0.017*
tumor grading	0.981	0.882-1.090	0.715
FIGO	1.024	1.003-1.046	0.028*
nodal status (pNX/0 vs. pN1)	1.655	0.803-3.415	0.172
positive nuclear co- expression of RIPK1 and RIPK3	0.386	0.187-0.797	0.010*

Significant independent factors for OS are indicated with asterisks. (*p < 0.05).

TABLE 7 Multivariate Cox regression analysis of cervical cancer patients (n = 250) and their clinical and pathological characteristics including nuclear RIPK1-RIPK3 co-expression regarding PFS.

covariate	hazard ratio	95% CI	p-value
patient's age (< 49 yrs vs. ≥ 49 yrs)	1.369	0.779-2.406	0.274
histological subtype	1.484	1.020-2.161	0.039*
tumor grading	0.985	0.906-1.071	0.719
FIGO	1.048	1.025-1.073	< 0.001**
nodal status (pNX/0 vs. pN1)	1.945	1.111-3.408	0.020*
positive nuclear co- expression of RIPK1 and RIPK3	0.521	0.296-0.917	0.024*

Significant independent factors for PFS are indicated with asterisks. (*p < 0.05, **p < 0.001).

3.2.5 Nuclear pMLKL expression is a positive prognosticator for PFS in the subgroup of grading G2 cervical cancer patients

In the subgroup of grading G2 cervical cancer, patients expressing nuclear pMLKL (IRS > 1) had a tendentially longer OS (p = 0.056) (as shown in Figure S1A). Furthermore, patients diagnosed with grading G2 cervical cancer expressing nuclear pMLKL (IRS > 0) had a significantly longer PFS (p = 0.043) (as shown in Figure S1B).

3.3 Cell viability and cell proliferation

3.3.1 C2 ceramide reduces cell viability and cell proliferation

In a previous study we could show that C2 ceramide can induce necroptosis in human luteal granulosa cells (36). To investigate C2 ceramide's effect on viability and cell proliferation in cervical cancer cells we conducted MTT and BrdU assays.

In MTT assay, CaSki, HeLa and SiHa cells showed a concentration-dependent decreasing viability after stimulation

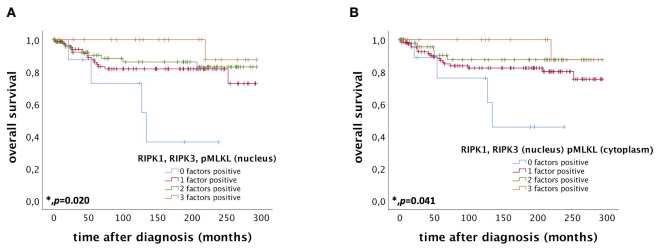

FIGURE 4
OS of patients diagnosed with cervical cancer correlated with co-expression of RIPK1, RIPK3, and pMLKL. **(A)** OS of patients diagnosed with cervical cancer correlated with co-expression of RIPK1, RIPK3, and pMLKL in the nucleus. Expression of all three factors (RIPK1, RIPK3, and pMLKL) (n = 22) in the nucleus was associated with longer OS in cervical cancer patients (p = 0.020) compared to patients expressing only two (n = 75), one (n = 97) or no factor (n = 9). **(B)** OS of patients diagnosed with cervical cancer correlated with co-expression of nuclear RIPK1 and RIPK3 and cytoplasmic pMLKL. Expression of all three factors (nuclear RIPK1, nuclear RIPK3 and cytoplasmic pMLKL) (n = 20) was associated with longer OS in cervical cancer patients (p = 0.041) compared to patients expressing only two (n = 51), one (n = 122) or no factor (n = 10).

TABLE 8 Multivariate Cox regression analysis of cervical cancer patients (n = 250) and their clinical and pathological characteristics including nuclear RIPK1-RIPK3-pMLKL co-expression regarding OS.

covariate	hazard ratio	95% CI	p-value
patient's age (< 49 yrs vs. ≥ 49 yrs)	1.995	0.911-4.368	0.084
histological subtype	1.849	1.188-2.878	0.006*
tumor grading	0.980	0.881-1.089	0.704
FIGO	1.022	1.000-1.044	0.052
nodal status (pNX/0 vs. pN1)	2.071	0.974-4.405	0.059
positive nuclear RIPK1, RIPK3, and pMLKL expression	0.573	0.340-0.964	0.036*

Significant independent factors for OS are indicated with asterisks. (*p < 0.05).

with 50μM, 100μM and 200μM C2 ceramide after 24h, 48h and 72h in comparison to the corresponding DMSO control (Figures 5A–C; Figure S3).

BrdU assay was performed for 48h and 72h because the effect of C2 ceramide in MTT assay was most present in these time frames. While stimulation of CaSki cells with C2 ceramide led to a significantly concentration-dependent decrease of cell proliferation after both 48h and 72h, cell proliferation in HeLa and SiHa cells was concentration-dependently inhibited only after 72h (Figures 5D–F; Figure S4).

3.3.2 Necrostatin-1 did not significantly inhibit the cell viability reductive effect of C2 ceramide

Nec-1 is an inhibitor of RIPK1. To identify the form of induced cell death caused by C2 ceramide, simultaneous stimulation of C2 ceramide and nec-1 or C2 ceramide and the pan-caspase inhibitor Z-VAD-fmk, respectively, was conducted. For that, CaSki, HeLa and SiHa cells were incubated with different concentrations of nec-1 (1μM, 5μM, 20μM and 50μM) followed by stimulation with 100μM C2 ceramide.

In HeLa cells, incubation with nec-1 did not lead to inhibition of the reduction of cell viability caused by C2 ceramide. Instead, cell viability decreased with higher concentration of nec-1. After 48h, co-stimulation of 100μM C2 ceramide and 50μM nec-1 showed a slight increase in CaSki and SiHa cell viability compared to the solvent control, which was insignificant. All other concentrations in all other time frames showed a decrease in cell viability (Figures 5G–I; Figure S5).

3.3.3 Z-VAD-fmk partially inhibited C2 ceramide's reductive effect on cell viability

CaSki, HeLa and SiHa cells were incubated with different concentrations of Z-VAD-fmk (1μM, 5μM, 20μM and 50μM) followed by stimulation with 100μM C2 ceramide.

In both CaSki and HeLa cells, co-stimulation of Z-VAD-fmk and C2 ceramide led to a significant concentration-dependent increase in viability after 72h. Co-stimulation of Z-VAD-fmk and C2 ceramide decreased cell viability in SiHa cells (Figures 5J–L).

3.4 Live-cell imaging showed necroptotic morphological changes in CaSki and HeLa cell lines stimulated with C2 ceramide

Live-cell imaging was performed over 72h after stimulation with C2 ceramide to investigate morphological changes. Incubation of CaSki and HeLa cells with C2 ceramide showed a visible reduction of confluency, and ballooning of the cells was observed. Treatment of SiHa cells with C2 ceramide did not have any visible effect on the morphology of cervical cancer cells.

3.5 C2 ceramide induced apoptosis and necroptosis in AnnexinV-FITC apoptosis staining followed by FACS analysis

To further specify the type of cell death induced by C2 ceramide, AnnexinV-FITC apoptosis staining followed by FACS

TABLE 9 Multivariate Cox regression analysis of cervical cancer patients (n = 250) and their clinical and pathological characteristics including nuclear RIPK1-RIPK3 and cytoplasmic pMLKL co-expression regarding OS.

covariate	hazard ratio	95% CI	p-value
patient's age (< 49 yrs vs. ≥ 49 yrs)	2.337	1.064-5.131	0.034*
histological subtype	1.959	1.258-3.051	0.003*
tumor grading	0.979	0.882-1.088	0.694
FIGO	1.023	1.001-1.045	0.041*
nodal status (pNX/0 vs. pN1)	1.770	0.823-3.807	0.144
positive nuclear RIPK1 and RIPK3 and cytoplasmic pMLKL expression	0.492	0.272-0.890	0.019*

Significant independent factors for OS are indicated with asterisks. (*p < 0.05).

analysis was performed after 72h stimulation with C2 ceramide (100µM). A significant percentual increase in apoptotic as well as in necrotic/intermediate (dying) cells compared to the respective control was observed in CaSki cells (Figures 6A, D). In SiHa cells, a significant increase in apoptotic but not in necrotic/intermediate (dying) cells was observed (Figures 6B, E). Treatment of HeLa cells with C2 ceramide did not show a significant percentual increase in apoptotic or necrotic/intermediate (dying) cells (Figures 6C, F).

3.6 RIPK3 expression in CaSki, HeLa and SiHa cells

The results of Western Blot showed that RIPK3 of expected size (~57kDa) was detected in all three cell lines examined (Figure S8).

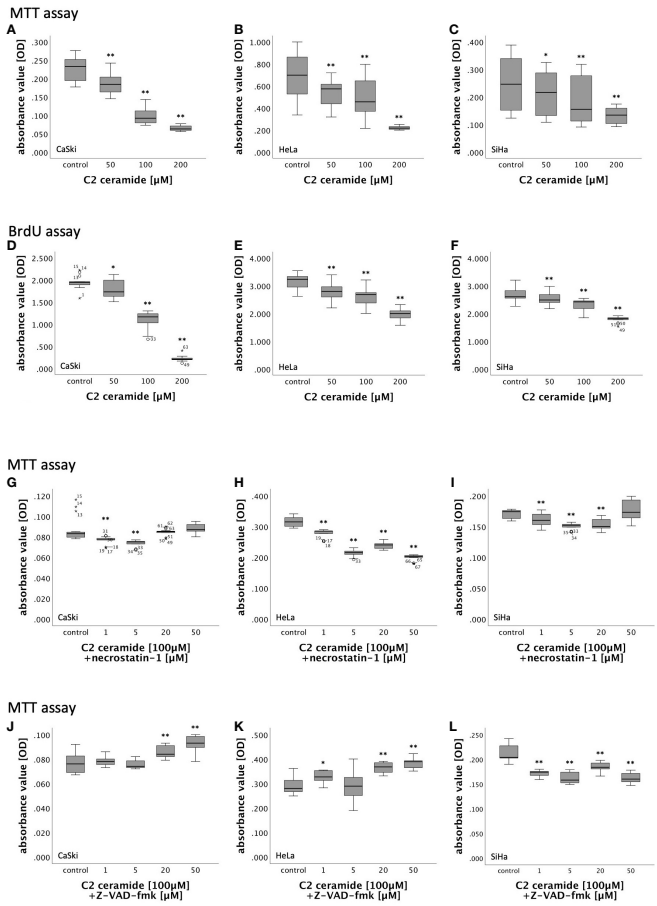

FIGURE 5
(A–F) MTT- and BrdU assay results of cervical cancer cell lines (CaSki, HeLa, SiHa) after 72h stimulation with C2 ceramide (50µM, 100µM, 200µM) compared to the respective DMSO control. **(G–L)** MTT assay results of cervical cancer cell lines (CaSki, HeLa, SiHa) after 48h stimulation with C2 ceramide (100µM) and necrostatin-1 (1µM, 5µM, 20µM and 50µM) compared to the respective DMSO control **(G–I)** and after 72h stimulation with C2 ceramide (100µM) and Z-VAD-fmk (1µM, 5µM, 20µM and 50µM) compared to the respective DMSO control **(J–L)** (for each concentration respectively control: n = 15, **p < 0.001, *p < 0.05).

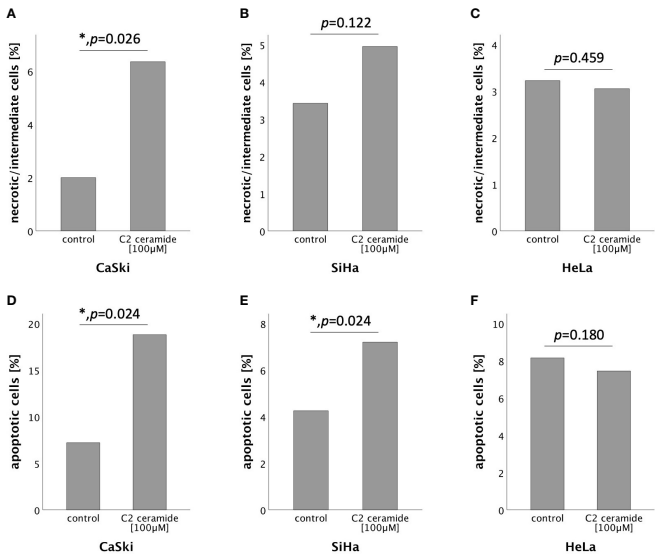

FIGURE 6
AnnexinV-FITC apoptosis staining followed by FACS comparing the percentual number of necrotic/intermediate cells of the control with the C2 ceramide treated cells **(A–C)**. AnnexinV-FITC apoptosis staining followed by FACS comparing the percentual number of apoptotic cells of the control with the C2 ceramide treated cells **(D–F)**.

4 Discussion

Necroptosis has been of growing interest in recent years. It was long considered as a "back-up" cell death mechanism in the TNFR1 pathway in case casp8 was blocked but since necroptosis can be induced not only *via* TNFR1 but also TNFR1-independently *via* ZBP1 and other receptors, the concept of necroptosis being only a "back-up" is being discussed (32). In the model of a hr-HPV-infected cell, this concept might still be of interest since the oncoprotein E6 binds to TNFR1 (44). Hr-HPV can block apoptosis and necroptosis (20, 45, 46). Inhibition of apoptosis through hr-HPV can either function *via* an increase of Bcl-2 and decrease of BAK caused by E6 and E7 (45) or by binding of the large isoform of E6 to procasp8, accelerating its degradation (46). Inhibition or degradation of casp8 prevents cleavage of RIPK1 and RIPK3 by the procasp8- $cFLIP_L$ heterodimer allowing autophosphorylation of RIPK3 and the induction of necroptosis (32). Since infection with hr-HPV also leads to downregulation of RIPK3 expression through a yet unknown mechanism, necroptosis is also blocked (20). The inhibition of necroptosis might enable infected cells to partially evade the effector mechanisms of the immune system and thereby facilitate a persistent infection with hr-HPV and ultimately, the progression of hr-HPV-induced lesions (20). Consistent with this study depicting necroptosis as a positive mechanism in cervical cancer, we found that patients with high nuclear RIPK3 expression, a key factor in the necroptotic pathway, had a significantly longer OS as well as PFS compared to patients with low expression of nuclear RIPK3. High nuclear RIPK3 expression was significantly associated with lower FIGO classification, low extent of the primary tumor (pT1) and negative lymph node status (pN0) in cervical cancer. This is supported by the findings indicating that RIPK3 is active in the nucleus and that nuclear RIPK3 is involved in necroptosis (47). Hence, we conclude that downregulation of RIPK3 *via* hr-HPV has a negative prognostic impact on OS and PFS in cervical cancer patients.

If necroptosis is induced *via* TNFR1, RIPK1 plays a key role in recruiting RIPK3 (21). In cervical cancer patients, expression of nuclear RIPK1 is an independent positive prognosticator for OS and PFS. Simultaneous expression of RIPK1 and RIPK3 in the nucleus is an independent positive prognosticator for OS and PFS further underlining a potential positive effect of necroptosis in cervical cancer patients.

RIPK3 phosphorylates MLKL in the nucleus (47), followed by translocation to intracellular and plasma membranes leading to disruption of membrane integrity and ultimately necroptotic cell death (26, 48, 49). In our study, we could show that expression of nuclear pMLKL is a positive prognosticator for PFS in patients diagnosed with G2 cervical cancer and that expression of cytoplasmic pMLKL is associated with negative regional lymph node involvement (pN0). While the expression of pMLKL seems to positively impact cervical cancer patients, high levels of pMLKL are associated with poor OS in esophageal and colon cancer (50). This

discrepancy in OS in different cancer types might be explained by different mechanisms of tumorigenesis with persistent hr-HPV infection being the leading cause of cervical cancer development (18). A reason for worse OS and PFS in cervical cancer patients not expressing the proteins necessary for necroptosis could be that E6 and E7 immortalize infected cells, targeting crucial regulators of proliferation and genomic stability (19), which might lead to the progression of HPV-induced lesions.

The presence of all three factors important for necroptosis (RIPK3, RIPK1, and pMLKL) is associated with a significantly longer OS compared to patients only expressing two, one or none of these factors. Since the expression of all three factors necessary for necroptosis is associated with longer OS, necroptosis could effectively regulate persistent hr-HPV infections and the progression of hr-HPV-induced lesions.

Persistent infection with hr-HPV not only leads to degradation of p53 through viral protein E6 (19) but also resists the induction of necroptosis in keratinocytes (20). p53 is an essential regulator of the cell cycle, acting as a tumor suppressor, and plays an important role in the regulation of necroptosis by leading to an increase of RIPK1 and RIPK3 through activation of necrosis-related factor (NRF) expression in cardiomyocytes (51). Consistent with these studies, we showed that expression of p53 correlated significantly with expression of nuclear and cytoplasmic RIPK1, nuclear RIPK3 and cytoplasmic pMLKL in cervical cancer tissue. Furthermore, E6 correlated negatively with nuclear and cytoplasmic pMLKL. hr-HPV oncoprotein E7 inactivates p21, an important cell cycle regulator and tumor suppressor (40). In this study, expression of p21 significantly correlated with most proteins relevant for necroptosis (nuclear and cytoplasmic RIPK1, nuclear RIPK3, nuclear pMLKL). The correlation of p53 and p21 with several proteins relevant for necroptosis indicates that insufficient degradation or insufficient inactivation of p53 and p21 through hr-HPV is associated with the preserved capability of necroptosis. We could also show strong positive correlation of all three examined factors (RIPK1, RIPK3, pMLKL) with each other. This could indicate that cervical cancer cells are capable of inducing necroptosis, specifically in those where RIPK3 is not downregulated.

Ceramides are biologically active sphingolipid metabolites that are important for cell death regulation in cancer cells, and the potential of ceramide analogs for treatment of ovarian cancer is currently being tested in several dose-escalating phase 1 clinical trials (33, 52). In human head and neck squamous cell carcinoma and human hepatocellular carcinoma, ceramide species are reduced (53, 54). Through induction of programmed cell death, ceramides, such as C2 ceramide, present as a potent tumor suppressor and, therefore, as a possible therapeutic strategy (55–58). In our study, C2 ceramide concentration-dependently reduced viability and proliferation in the cervical cancer cell lines CaSki, HeLa, and SiHa leading to the assumption that cell death can be induced by C2 ceramide in cervical cancer cells. Morphological changes after stimulation with C2 ceramide were evaluated using live-cell imaging. In CaSki and HeLa cells, signs typical for necro(pto)tic cell death, such as ballooning and reduction of confluency, could be detected after stimulation with C2 ceramide, whereas treatment of SiHa cells did not have any visible effects. To further identify the form of induced cell death, we tried to neutralize C2 ceramide's effect by simultaneous stimulation of C2 ceramide together with the RIPK1 inhibitor nec-1 or the pan-caspase inhibitor Z-VAD-fmk. Nec-1 did not significantly reverse C2 ceramide's effect on cell viability but showed a tendency (p=0.108) in SiHa cells when co-stimulated with 50nM of nec-1 for 48h. This is in favor of a necroptotic event. Z-VAD-fmk significantly inhibited C2 ceramide's effect in CaSki and HeLa cells after 72h.

Feoktistova et al. (2011) postulated that HeLa cells lack basal RIPK3 expression (59). We could show that HeLa cells, as well as CaSki and SiHa cells, express sufficient levels of RIPK3, potentially enabling CaSki, HeLa and SiHa cells to necroptosis. AnnexinV-FITC apoptosis staining followed by Flow Cytometry proved a significant increase in apoptotic CaSki and SiHa cells after treatment with C2 ceramide compared to the control. It also showed a significant increase in necrotic/intermediate (dying) CaSki cells compared to the control. C2 ceramide induces necroptosis in human luteal granulosa cells (36). It can also induce apoptosis in human malignant glioma cells (58) and human colon carcinoma cells (60). In head and neck squamous cell carcinoma, both necroptosis and apoptosis are induced by C2 ceramide (57). It is possible that C2 ceramide induces cell death independently of RIPK1 and that this is the reason why simultaneous stimulation of C2 ceramide and the RIPK1 inhibitor nec-1 did not show any inhibitory effects of C2 ceramide in the MTT assay. Taken together, these are indicators that C2 ceramide induces both necroptosis and apoptosis in the two cervical cancer cell lines CaSki and HeLa. Further studies are required to identify the exact mechanism by which C2 ceramide induces cell death.

In conclusion, this study showed that RIPK1 and RIPK3 correlated with longer OS and PFS in cervical cancer patients and can therefore be described as positive prognosticators for cervical cancer. pMLKL was associated with longer PFS in the subgroup of G2 grading. These results comply with the current understanding of hr-HPV infection, which can inhibit programmed cell deaths to evade effector mechanisms of the immune system and thereby potentially promote tumorigenesis (20, 45, 46). This study further elucidated the effect of C2 ceramide on cell viability and cell proliferation. Consistent with *in vitro* studies in other cancer cell lines (36, 57, 58, 60), C2 ceramide reduced cell viability and cell proliferation in cervical cancer cell lines. AnnexinV-FITC apoptosis staining followed by FACS analysis supported the results indicating that cell viability is reduced through the induction of both apoptosis and necroptosis.

Conflicts of interest

The authors declare that the research was conducted in the absence of any commercial or financial relationships that could be construed as a potential conflict of interest.

Data availability statement

The original contributions presented in the study are included in the article/Supplementary Material. Further inquiries can be directed to the corresponding author.

Ethics statement

The studies involving human participants were reviewed and approved by ethics committee of Ludwig-Maximilians University of Munich. Written informed consent for participation was not required for this study in accordance with the national legislation and the institutional requirements.

Author contributions

AV, AM and UJ designed and conceived the project, provided the concept, edited the manuscript, and supervised the research. TV performed most experiments, all statistical evaluation and wrote the manuscript. VK and SJ performed experiments and contributed to editing of the manuscript. ES, KB, KE, DM, AT, NT and SM contributed to the editing of the manuscript. All authors contributed to the article and approved the submitted version.

Funding

TV and AV have received funds for this study from the structured promotion program of the Ludwig-Maximilians University of Munich, "Molecular and clinically translational Medicine".

Acknowledgments

The authors thank Christina Kuhn, Carola Herrmann, Simone Hofmann, Martina Rahmeh and Michelle Schneider for their excellent technical assistance. This work was supported by the structured promotion program of Ludwig-Maximilians University of Munich, "Molecular and clinically translational Medicine". The funder had no influence in study design, data collection and analysis, decision to publish or preparation of the manuscript.

Conflict of interest

The authors declare that the research was conducted in the absence of any commercial or financial relationships that could be construed as a potential conflict of interest.

Publisher's note

Supplementary material

The Supplementary Material for this article can be found online at: https://www.frontiersin.org/articles/10.3389/fonc.2023.1110939/full#supplementary-material

References

1. Degterev A, Huang Z, Boyce M, Li Y, Jagtap P, Mizushima N, et al. Chemical inhibitor of nonapoptotic cell death with therapeutic potential for ischemic brain injury. *Nat Chem Biol* (2005) 1(2):112–9. doi: 10.1038/nchembio711

2. Bailey LJ, Alahari S, Tagliaferro A, Post M, Caniggia I. Augmented trophoblast cell death in preeclampsia can proceed *via* ceramide-mediated necroptosis. *Cell Death Dis* (2017) 8(2):e2590. doi: 10.1038/cddis.2016.483

3. Mocarski ES, Upton JW, Kaiser WJ. Viral infection and the evolution of caspase 8-regulated apoptotic and necrotic death pathways. *Nat Rev Immunol* (2011) 12(2):79–88. doi: 10.1038/nri3131

4. Linkermann A, Green DR. Necroptosis. *N Engl J Med* (2014) 370(5):455–65. doi: 10.1056/NEJMra1310050

5. Lin J, Li H, Yang M, Ren J, Huang Z, Han F, et al. A role of RIP3-mediated macrophage necrosis in atherosclerosis development. *Cell Rep* (2013) 3(1):200–10. doi: 10.1016/j.celrep.2012.12.012

6. Naito MG, Xu D, Amin P, Lee J, Wang H, Li W, et al. Sequential activation of necroptosis and apoptosis cooperates to mediate vascular and neural pathology in stroke. *Proc Natl Acad Sci U S A* (2020) 117(9):4959–70. doi: 10.1073/pnas.1916427117

7. Degterev A, Hitomi J, Germscheid M, Ch'en IL, Korkina O, Teng X, et al. Identification of RIP1 kinase as a specific cellular target of necrostatins. *Nat Chem Biol* (2008) 4(5):313–21. doi: 10.1038/nchembio.83

8. Smith CC, Davidson SM, Lim SY, Simpkin JC, Hothersall JS, Yellon DM. Necrostatin: a potentially novel cardioprotective agent? *Cardiovasc Drugs Ther* (2007) 21(4):227–33. doi: 10.1007/s10557-007-6035-1

9. Linkermann A, Brasen JH, Himmerkus N, Liu S, Huber TB, Kunzendorf U, et al. Rip1 (receptor-interacting protein kinase 1) mediates necroptosis and contributes to renal ischemia/reperfusion injury. *Kidney Int* (2012) 81(8):751–61. doi: 10.1038/ki.2011.450

10. Wu J, Huang Z, Ren J, Zhang Z, He P, Li Y, et al. Mlkl knockout mice demonstrate the indispensable role of mlkl in necroptosis. *Cell Res* (2013) 23(8):994–1006. doi: 10.1038/cr.2013.91

11. Günther C, Martini E, Wittkopf N, Amann K, Weigmann B, Neumann H, et al. Caspase-8 regulates TNF-α-induced epithelial necroptosis and terminal ileitis. *Nature* (2011) 477(7364):335–9. doi: 10.1038/nature10400

12. Welz PS, Wullaert A, Vlantis K, Kondylis V, Fernandez-Majada V, Ermolaeva M, et al. FADD prevents RIP3-mediated epithelial cell necrosis and chronic intestinal inflammation. *Nature* (2011) 477(7364):330–4. doi: 10.1038/nature10273

13. Werts AD, Fulton WB, Ladd MR, Saad-Eldin A, Chen YX, Kovler ML, et al. A novel role for necroptosis in the pathogenesis of necrotizing enterocolitis. *Cell Mol Gastroenterol Hepatol* (2020) 9(3):403–23. doi: 10.1016/j.jcmgh.2019.11.002

14. Najafov A, Chen H, Yuan J. Necroptosis and cancer. *Trends Cancer* (2017) 3(4):294–301. doi: 10.1016/j.trecan.2017.03.002

15. World Health Organization. *Cervical cancer* . Available at: https://www.who.int/news-room/fact-sheets/detail/cervical-cancer.

16. Leitlinienprogramm Onkologie (Deutsche Krebsgesellschaft, Deutsche Krebshilfe, AWMF). *S3-leitlinie diagnostik, therapie und nachsorge der patientin mit zervixkarzinom, Lang* . Available at: https://www.leitlinienprogramm-onkologie.de/leitlinien/zervixkarzinom/.

17. Lei J, Ploner A, Elfström KM, Wang J, Roth A, Fang F, et al. HPV vaccination and the risk of invasive cervical cancer. *N Engl J Med* (2020) 383(14):1340–8. doi: 10.1056/NEJMoa1917338

18. Bosch FX, Lorincz A, Muñoz N, Meijer CJ, Shah KV. The causal relation between human papillomavirus and cervical cancer. *J Clin Pathol* (2002) 55(4):244–65. doi: 10.1136/jcp.55.4.244

19. Moody CA, Laimins LA. Human papillomavirus oncoproteins: pathways to transformation. *Nat Rev Cancer* (2010) 10(8):550–60. doi: 10.1038/nrc2886

20. Ma W, Tummers B, van Esch EM, Goedemans R, Melief CJ, Meyers C, et al. Human papillomavirus downregulates the expression of IFITM1 and RIPK3 to escape from IFNgamma- and TNFalpha-mediated antiproliferative effects and necroptosis. *Front Immunol* (2016) 7:496. doi: 10.3389/fimmu.2016.00496

21. Jorgensen I, Rayamajhi M, Miao EA. Programmed cell death as a defence against infection. *Nat Rev Immunol* (2017) 17(3):151–64. doi: 10.1038/nri.2016.147

22. Dillon CP, Weinlich R, Rodriguez DA, Cripps JG, Quarato G, Gurung P, et al. RIPK1 blocks early postnatal lethality mediated by caspase-8 and RIPK3. *Cell* (2014) 157(5):1189–202. doi: 10.1016/j.cell.2014.04.018

23. Galluzzi L, Vitale I, Aaronson SA, Abrams JM, Adam D, Agostinis P, et al. Molecular mechanisms of cell death: recommendations of the nomenclature committee on cell death 2018. *Cell Death Differ* (2018) 25(3):486–541. doi: 10.1038/s41418-017-0012-4

24. Kaiser WJ, Upton JW, Mocarski ES. Viral modulation of programmed necrosis. *Curr Opin Virol* (2013) 3(3):296–306. doi: 10.1016/j.coviro.2013.05.019

25. Kaczmarek A, Vandenabeele P, Krysko DV. Necroptosis: the release of damage-associated molecular patterns and its physiological relevance. *Immunity* (2013) 38 (2):209–23. doi: 10.1016/j.immuni.2013.02.003

26. Wang H, Sun L, Su L, Rizo J, Liu L, Wang LF, et al. Mixed lineage kinase domain-like protein MLKL causes necrotic membrane disruption upon phosphorylation by RIP3. *Mol Cell* (2014) 54(1):133–46. doi: 10.1016/j.molcel.2014.03.003

27. Cho YS, Challa S, Moquin D, Genga R, Ray TD, Guildford M, et al. Phosphorylation-driven assembly of the RIP1-RIP3 complex regulates programmed necrosis and virus-induced inflammation. *Cell* (2009) 137(6):1112–23. doi: 10.1016/j.cell.2009.05.037

28. He S, Wang L, Miao L, Wang T, Du F, Zhao L, et al. Receptor interacting protein kinase-3 determines cellular necrotic response to TNF-alpha. *Cell* (2009) 137(6):1100–11. doi: 10.1016/j.cell.2009.05.021

29. Zhang DW, Shao J, Lin J, Zhang N, Lu BJ, Lin SC, et al. RIP3, an energy metabolism regulator that switches TNF-induced cell death from apoptosis to necrosis. *Science* (2009) 325(5938):332–6. doi: 10.1126/science.1172308

30. Tummers B, Green DR. Caspase-8: regulating life and death. *Immunol Rev* (2017) 277(1):76–89. doi: 10.1111/imr.12541

31. Bianchi K, Meier P. A tangled web of ubiquitin chains: breaking news in TNF-R1 signaling. *Mol Cell* (2009) 36(5):736–42. doi: 10.1016/j.molcel.2009.11.029

32. Tummers B, Green DR. The evolution of regulated cell death pathways in animals and their evasion by pathogens. *Physiol Rev* (2022) 102(1):411–54. doi: 10.1152/physrev.00002.2021

33. Ogretmen B, Hannun YA. Biologically active sphingolipids in cancer pathogenesis and treatment. *Nat Rev Cancer* (2004) 4(8):604–16. doi: 10.1038/nrc1411

34. Bieberich E, Kawaguchi T, Yu RK. N-acylated serinol is a novel ceramide mimic inducing apoptosis in neuroblastoma cells. *J Biol Chem* (2000) 275(1):177–81. doi: 10.1074/jbc.275.1.177

35. Struckhoff AP, Bittman R, Burow ME, Clejan S, Elliott S, Hammond T, et al. Novel ceramide analogs as potential chemotherapeutic agents in breast cancer. *J Pharmacol Exp Ther* (2004) 309(2):523–32. doi: 10.1124/jpet.103.062760

36. Bagnjuk K, Stockl JB, Frohlich T, Arnold GJ, Behr R, Berg U, et al. Necroptosis in primate luteolysis: a role for ceramide. *Cell Death Discovery* (2019) 5:67. doi: 10.1038/s41420-019-0149-7

37. Remmele W, Stegner HE. [Recommendation for uniform definition of an immunoreactive score (IRS) for immunohistochemical estrogen receptor detection (ER-ICA) in breast cancer tissue]. *Pathologe* (1987) 8(3):138–40.

38. Bagnjuk K, Kast VJ, Tiefenbacher A, Kaseder M, Yanase T, Burges A, et al. Inhibitor of apoptosis proteins are potential targets for treatment of granulosa cell tumors - implications from studies in KGN. *J Ovarian Res* (2019) 12(1):76. doi: 10.1186/s13048-019-0549-6

39. Blohberger J, Kunz L, Einwang D, Berg U, Berg D, Ojeda SR, et al. Readthrough acetylcholinesterase (AChE-r) and regulated necrosis: pharmacological targets for the regulation of ovarian functions? *Cell Death Dis* (2015) 6(3):e1685. doi: 10.1038/cddis.2015.51

40. Shin MK, Balsitis S, Brake T, Lambert PF. Human papillomavirus E7 oncoprotein overrides the tumor suppressor activity of p21Cip1 in cervical carcinogenesis. *Cancer Res* (2009) 69(14):5656–63. doi: 10.1158/0008-5472.CAN-08-3711

41. *Kaplan-Meier Plotter* . Available at: https://kmplot.com/analysis/ (Accessed 08th January 2023).

42. Yang Z, Li J, Tang Y, Zou L. Identification and validation a necroptosis-related prognostic signature in cervical cancer. *Reprod Sci* (2022). doi: 10.1007/s43032-022-01155-y

43. Sun K, Huang C, Li JZ, Luo ZX. Identification of a necroptosis-related prognostic gene signature associated with tumor immune microenvironment in cervical carcinoma and experimental verification. *World J Surg Oncol* (2022) 20 (1):342. doi: 10.1186/s12957-022-02802-z

44. Filippova M, Song H, Connolly JL, Dermody TS, Duerksen-Hughes PJ. The human papillomavirus 16 E6 protein binds to tumor necrosis factor (TNF) R1 and protects cells from TNF-induced apoptosis. *J Biol Chem* (2002) 277(24):21730–9. doi: 10.1074/jbc.M200113200

45. Liu HC, Chen GG, Vlantis AC, Tse GM, Chan AT, van Hasselt CA. Inhibition of apoptosis in human laryngeal cancer cells by E6 and E7 oncoproteins of human papillomavirus 16. *J Cell Biochem* (2008) 103(4):1125–43. doi: 10.1002/jcb.21490

46. Filippova M, Johnson MM, Bautista M, Filippov V, Fodor N, Tungteakkhun SS, et al. The large and small isoforms of human papillomavirus type 16 E6 bind to and differentially affect procaspase 8 stability and activity. *J Virol* (2007) 81(8):4116–29. doi: 10.1128/JVI.01924-06

47. Weber K, Roelandt R, Bruggeman I, Estornes Y, Vandenabeele P. Nuclear RIPK3 and MLKL contribute to cytosolic necrosome formation and necroptosis. *Commun Biol* (2018) 1:6. doi: 10.1038/s42003-017-0007-1

48. Cai Z, Jitkaew S, Zhao J, Chiang HC, Choksi S, Liu J, et al. Plasma membrane translocation of trimerized MLKL protein is required for TNF-induced necroptosis. *Nat Cell Biol* (2014) 16(1):55–65. doi: 10.1038/ncb2883

49. Dondelinger Y, Declercq W, Montessuit S, Roelandt R, Goncalves A, Bruggeman I, et al. MLKL compromises plasma membrane integrity by binding to phosphatidylinositol phosphates. *Cell Rep* (2014) 7(4):971–81. doi: 10.1016/j.celrep.2014.04.026

50. Liu X, Zhou M, Mei L, Ruan J, Hu Q, Peng J, et al. Key roles of necroptotic factors in promoting tumor growth. *Oncotarget* (2016) 7(16):22219–33. doi: 10.18632/oncotarget.7924

51. Wang K, Liu F, Liu CY, An T, Zhang J, Zhou LY, et al. The long noncoding RNA NRF regulates programmed necrosis and myocardial injury during ischemia and reperfusion by targeting miR-873. *Cell Death Differ* (2016) 23(8):1394–405. doi: 10.1038/cdd.2016.28

52. Zhang X, Kitatani K, Toyoshima M, Ishibashi M, Usui T, Minato J, et al. Ceramide nanoliposomes as a MLKL-dependent, necroptosis-inducing, chemotherapeutic reagent in ovarian cancer. *Mol Cancer Ther* (2018) 17(1):50–9. doi: 10.1158/1535-7163.MCT-17-0173

53. Karahatay S, Thomas K, Koybasi S, Senkal CE, Elojeimy S, Liu X, et al. Clinical relevance of ceramide metabolism in the pathogenesis of human head and neck squamous cell carcinoma (HNSCC): attenuation of C(18)-ceramide in HNSCC tumors correlates with lymphovascular invasion and nodal metastasis. *Cancer Lett* (2007) 256(1):101–11. doi: 10.1016/j.canlet.2007.06.003

54. Krautbauer S, Meier EM, Rein-Fischboeck L, Pohl R, Weiss TS, Sigruener A, et al. Ceramide and polyunsaturated phospholipids are strongly reduced in human hepatocellular carcinoma. *Biochim Biophys Acta* (2016) 1861(11):1767–74. doi: 10.1016/j.bbalip.2016.08.014

55. Morad SA, Cabot MC. Ceramide-orchestrated signalling in cancer cells. *Nat Rev Cancer* (2013) 13(1):51–65. doi: 10.1038/nrc3398

56. Obeid LM, Linardic CM, Karolak LA, Hannun YA. Programmed cell death induced by ceramide. *Science* (1993) 259(5102):1769–71. doi: 10.1126/science.8456305

57. Zhu W, Wang X, Zhou Y, Wang H. C2-ceramide induces cell death and protective autophagy in head and neck squamous cell carcinoma cells. *Int J Mol Sci* (2014) 15(2):3336–55. doi: 10.3390/ijms15023336

58. Wagenknecht B, Roth W, Gulbins E, Wolburg H, Weller M. C2-ceramide signaling in glioma cells: synergistic enhancement of CD95-mediated, caspase-dependent apoptosis. *Cell Death Differ* (2001) 8(6):595–602. doi: 10.1038/sj.cdd.4400848

59. Feoktistova M, Geserick P, Kellert B, Dimitrova DP, Langlais C, Hupe M, et al. cIAPs block ripoptosome formation, a RIP1/caspase-8 containing intracellular cell death complex differentially regulated by cFLIP isoforms. *Mol Cell* (2011) 43(3):449–63. doi: 10.1016/j.molcel.2011.06.011

60. Zhang XF, Li BX, Dong CY, Ren R. Apoptosis of human colon carcinoma HT-29 cells induced by ceramide. *World J Gastroenterol* (2006) 12(22):3581–4. doi: 10.3748/wjg.v12.i22.3581

6. Publikation II

Titel

Prognostic Impact of Heat Shock Protein 90 Expression in Women Diagnosed with Cervical Cancer

Autoren

Tilman LR Vogelsang, Elisa Schmoeckel, Nicole Elisabeth Topalov, Franziska Ganster, Sven Mahner, Udo Jeschke, Aurelia Vattai

Journal

Int J Mol Sci. 2024 Jan 26; 25(3):1571.

doi: 10.3390/ijms25031571

Abstract

Heat Shock Protein 90 (HSP90), a major molecular chaperone, plays a crucial role in cell function by folding and stabilizing proteins and maintaining proteostasis. This study aimed to elucidate the prognostic impact of HSP90 in cervical cancer. We analyzed HSP90 expression using immunohistochemistry in cervical cancer tissue microarrays from 250 patients. This study investigated correlations between HSP90 expression levels and key clinical outcomes, including overall survival (OS), progression-free survival (PFS), and FIGO classification. The statistical analyses employed included the Kruskal–Wallis-H test, log-rank (Mantel–Cox), and Cox regression. Our findings indicate that high nuclear HSP90 expression is associated with improved OS, while high cytoplasmic HSP90 expression correlates with better PFS and a lower FIGO classification in cervical squamous cell carcinoma patients. These results suggest that HSP90 could serve as a positive prognostic factor in patients diagnosed with cervical squamous cell carcinoma, underlining its potential as a biomarker for patient prognosis and as a target for therapeutic strategies.

International Journal of
Molecular Sciences

MDPI

Article

Prognostic Impact of Heat Shock Protein 90 Expression in Women Diagnosed with Cervical Cancer

Tilman L. R. Vogelsang [1,2], Elisa Schmoeckel [3], Nicole Elisabeth Topalov [1], Franziska Ganster [1], Sven Mahner [1], Udo Jeschke [1,4] and Aurelia Vattai [1,*]

[1] Department of Obstetrics and Gynecology, University Hospital, LMU Munich, 80337 Munich, Germany
[2] Department of Obstetrics and Gynecology, Medical University of Graz, 8010 Graz, Austria
[3] Institute of Pathology, Faculty of Medicine, LMU Munich, 80337 Munich, Germany
[4] Department of Obstetrics and Gynecology, University Hospital Augsburg, 86156 Augsburg, Germany
* Correspondence: aurelia.vattai@med.uni-muenchen.de; Tel.: +49-89-4400-74775

Abstract: Heat Shock Protein 90 (HSP90), a major molecular chaperone, plays a crucial role in cell function by folding and stabilizing proteins and maintaining proteostasis. This study aimed to elucidate the prognostic impact of HSP90 in cervical cancer. We analyzed HSP90 expression using immunohistochemistry in cervical cancer tissue microarrays from 250 patients. This study investigated correlations between HSP90 expression levels and key clinical outcomes, including overall survival (OS), progression-free survival (PFS), and FIGO classification. The statistical analyses employed included the Kruskal–Wallis-H test, log-rank (Mantel–Cox), and Cox regression. Our findings indicate that high nuclear HSP90 expression is associated with improved OS, while high cytoplasmic HSP90 expression correlates with better PFS and a lower FIGO classification in cervical squamous cell carcinoma patients. These results suggest that HSP90 could serve as a positive prognostic factor in patients diagnosed with cervical squamous cell carcinoma, underlining its potential as a biomarker for patient prognosis and as a target for therapeutic strategies.

Keywords: HSP90; chaperone; cervical cancer; human papillomavirus; necroptosis; programmed cell death

Citation: Vogelsang, T.L.R.; Schmoeckel, E.; Topalov, N.E.; Ganster, F.; Mahner, S.; Jeschke, U.; Vattai, A. Prognostic Impact of Heat Shock Protein 90 Expression in Women Diagnosed with Cervical Cancer. *Int. J. Mol. Sci.* **2024**, *25*, 1571. https://doi.org/10.3390/ijms25031571

Academic Editor: Robert Garfield

Received: 29 December 2023
Revised: 21 January 2024
Accepted: 24 January 2024
Published: 26 January 2024

1. Introduction

Cervical cancer remains a significant global health challenge, with roughly 604,000 new cases and approximately 342,000 related deaths in 2020, ranking it as the fourth most common cancer among women worldwide [1]. This burden, however, is unevenly distributed, with a higher prevalence in developing countries due to disparities in access to screening, vaccination, and treatment. The main histological subtypes of cervical cancer are squamous cell carcinoma (accounting for about 80% of cases), adenocarcinoma (15–20%), and the less common adenosquamous carcinoma [2,3]. A key factor in the majority of cervical cancer cases is persistent infection with high-risk human papillomavirus (hr-HPV) [4], highlighting the importance of preventative measures such as HPV vaccination and effective screening programs. Upon intracellular hr-HPV replication, the viral oncoproteins E6 and E7 are expressed and promote genomic instability, hyperproliferation and immortalization, block apoptosis and disturb the cell cycle [5]. Hr-HPV also suppresses the induction of necroptosis [6]. Necroptosis, a regulated form of cell death, is critically dependent on the proteins RIPK3 (receptor-interacting serin/threonine-protein kinase 3), MLKL (mixed lineage kinase domain-like protein), and, in some cases, the kinase activity of RIPK1 (receptor-interacting serin/threonine-protein kinase 1) [7]. In the context of cervical cancer, hr-HPV can interfere with this cell death pathway. This interference occurs through the downregulation of RIPK3, leading to a partial evasion of the immune responses. This evasion potentially facilitates the progression of hr-HPV induced lesions [6]. Furthermore, research has demonstrated that the low expression of RIPK3 and RIPK1, as observed

through immunohistochemical staining, is associated with a worse prognosis in cervical cancer patients. Specifically, these proteins have been identified as positive prognostic indicators for both overall survival (OS) and progression-free survival (PFS) [8].

Over the last three decades, there has been a notable decrease in the incidence and mortality rates of cervical cancer in several regions, largely attributable to the effectiveness of the Papanicolaou (Pap) smear test, the introduction of HPV vaccination, and advances in treatment programs [3,9,10]. However, it is important to recognize that this trend is primarily observed in Western countries with organized screening programs. In contrast, the majority of cervical cancer cases occur in developing countries, where access to such screening, vaccination, and advanced treatments is often limited [9,11]. The global impact of HPV vaccination, while promising, may not yet be fully realized due to its relatively recent implementation and varying coverage levels worldwide. Additionally, the introduction of HPV testing as a primary screening method has shown potential for further improving early detection, especially in countries where it has been integrated into national screening programs. This development, however, highlights the disparities in access to advanced screening techniques between developed and developing countries.

Molecular chaperones are defined as any protein that stabilizes, interacts or helps a non-native protein to gain its native conformation without being present in its final structure [12]. They are crucial for protein quality control and proteome homeostasis, also known as proteostasis, ensuring that proteins are folded correctly and functional [13]. Chaperones are upregulated in stress conditions, such as a sudden rise in temperature (hence, the term "heat shock protein"), but are also important under physiological conditions [14]. Deficiencies in proteostasis are associated with the progression and manifestation of various diseases including cancer, cardiovascular diseases, neurodegeneration, dementia and type 2 diabetes [15]. Chaperones are classified according to their molecular weight (HSP40, HSP60, HSP70, HSP90, HSP100 and small HSPs) [15].

Heat shock protein 90 (HSP90) regulates the conformation, activation, function and stability of a large number of so-called 'client proteins', including transcription factors and kinases [16]. It can assist protein folding, the assembly of multiprotein complexes or the binding of a ligand to its target or receptor [14]. HSP90 is also involved in several cellular processes including regulated cell death, DNA repair, development, and immune response [14,17]. During necroptosis, a complex of HSP90 and its co-chaperone cell division cycle 37 (CDC37) is required for the activation of RIPK3 [18]. Furthermore, the inhibition or disruption of HSP90 leads to the inhibition of necroptosis and the degradation of client proteins relevant to necroptosis, such as RIPK1 [19,20], RIPK3 [19,21] and MLKL [21,22].

The aim of this study was to evaluate the prognostic impact of HSP90 in cervical carcinoma patients. This focus stems from the known importance of HSP90 in the necroptosis process [17], coupled with evidence that the expression of necroptosis-related proteins is associated with improved OS and PFS in these patients and that expression of proteins relevant to necroptosis is associated with better OS and PFS [8].

2. Results

2.1. Correlation of HSP90 with Histology, Grading and TNM- and FIGO-Classification

Cytoplasmic HSP90 expression was significantly higher in adenocarcinoma and adenosqamous carcinoma (median IRS 3) compared to squamous cell carcinoma (median IRS 2) ($p = 0.040$) (as depicted in Figure 1a–d).

High cytoplasmic HSP90 expression showed a significant correlation with the pN0 status ($p = 0.003$), exhibiting a median Immuno-Reactive Score (IRS) of 2, in contrast to patients with the pN1 status, who had a median IRS of 0 (as depicted in Figure 2a). High cytoplasmic HSP90 expression was also found to significantly correlate with a low FIGO classification ($p = 0.004$), exhibiting a median IRS of 2. This contrasts with patients who have a high FIGO classification, demonstrating a median IRS of 0 (as depicted in Figure 2b).

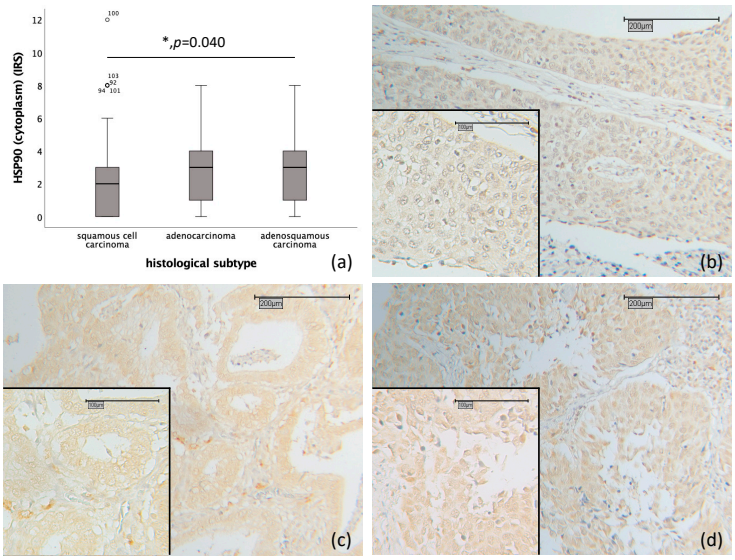

Figure 1. Correlation of cytoplasmic HSP90 expression with histological subtype in cervical carcinoma (p = 0.040). (**a**) Boxplot of cytoplasmic HSP90 expression and histological subtype in cervical carcinoma. (**b**) Cervical carcinoma and squamous cell carcinoma (n = 180) with a cytoplasmic HSP90 IRS of 1; magnification ×10 and ×25 in the inset. (**c**) Cervical carcinoma and adenocarcinoma (n = 32) with a cytoplasmic HSP90 IRS of 4; magnification ×10 and ×25 in the inset. (**d**) Cervical carcinoma and adenosquamous carcinoma (n = 13) with a cytoplasmic HSP90 IRS of 4; magnification ×10 and ×25 in the inset.

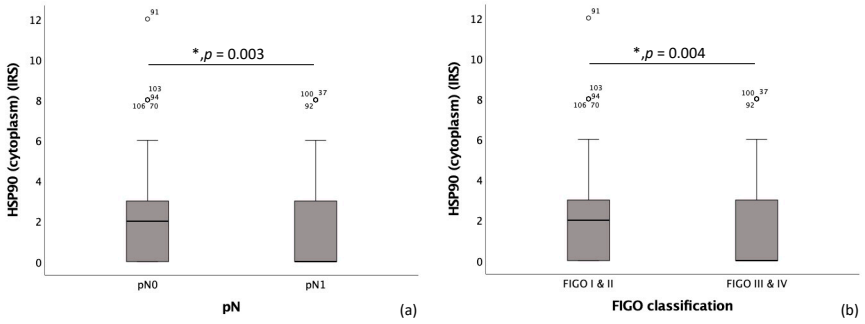

Figure 2. Correlation of HSP90 with pN and FIGO-classification. (**a**) Boxplot of cytoplasmic HSP90 expression and regional lymph node status (pN) in cervical carcinoma (p = 0.003); median IRS of cytoplasmic HSP90 expression in pN0 is 2 (n = 125) and in pN1 is 0 (n = 94). (**b**) Boxplot of cytoplasmic HSP90 expression and FIGO classification in cervical carcinoma (p = 0.004); median IRS of cytoplasmic HSP90 expression in FIGO I and II is 2 (n = 125) and in FIGO III and IV is 0 (n = 125).

2.2. High Nuclear HSP90 Expression as a Positive Prognostic Factor for OS in Patients Diagnosed with Cervical Squamous Cell Carcinoma

Patients with cervical squamous cell carcinoma exhibiting high nuclear HSP90 expression (IRS > 2) demonstrated a significantly better OS compared to those with low nuclear HSP90 expression (p = 0.012), as illustrated in Figure 3. Further, a multivariate Cox regression analysis, conducted on a cohort of 174 cervical squamous cell carcinoma patients, identified nuclear HSP90 expression as an independent prognostic factor for OS, as detailed in Table 1.

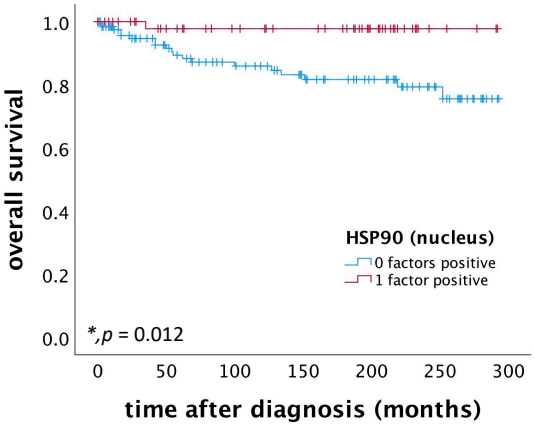

Figure 3. OS of patients diagnosed with cervical squamous cell carcinoma correlated with nuclear HSP90. Nuclear HSP90 expression (n = 53) is associated with a better OS in cervical squamous cell carcinoma patients compared to patients not expressing nuclear HSP90 (n = 127) (p = 0.012).

Table 1. Multivariate Cox regression analysis of cervical squamous cell carcinoma patients (n = 174) and their clinical and pathological characteristics including the nuclear HSP90 expression regarding OS. Significant independent factors for OS are indicated with asterisks. (* $p < 0.05$).

Covariate	Hazard Ratio	95% CI	*p*-Value
patient's age (<49 years vs. ≥49 years)	1.372	0.540–3.488	0.507
tumor grading	0.986	0.895–1.086	0.769
extent of the primary tumor [7]	2.510	1.048–6.015	0.039 *
nodal status (pNX/0 vs. pN1)	2.311	0.813–6.570	0.116
FIGO classification	0.407	0.171–0.971	0.043 *
positive nuclear HSP90 expression	0.127	0.017–0.957	0.045 *

2.3. High Cytoplasmic HSP90 Expression Correlates with Improved PFS in Patients Diagnosed with Cervical Squamous Cell Carcinoma

Patients diagnosed with cervical squamous cell carcinoma and exhibiting high cytoplasmic HSP90 expression (IRS > 3) demonstrated a significantly improved PFS compared to those with low cytoplasmic HSP90 expression (p = 0.033), as depicted in Figure 4. Multivariate Cox regression analysis, conducted on a cohort of 168 patients with cervical squamous cell carcinoma, identified high cytoplasmic HSP90 expression as an independent positive prognostic factor for PFS, as detailed in Table 2.

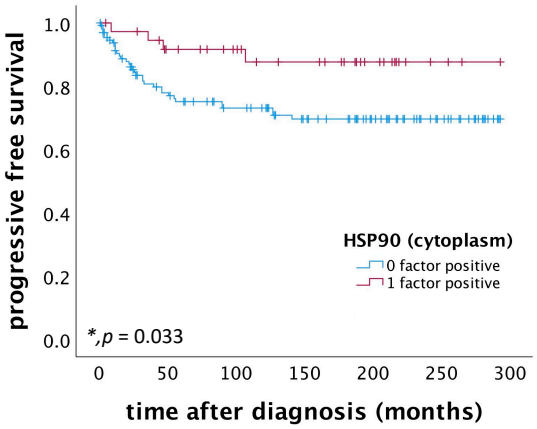

Figure 4. PFS in patients diagnosed with cervical squamous cell carcinoma was found to be associated with cytoplasmic HSP90 expression. Specifically, patients exhibiting high cytoplasmic HSP90 expression (n = 38) demonstrated significantly improved PFS compared to those with low cytoplasmic HSP90 expression (n = 133) (p = 0.033).

Table 2. Multivariate Cox regression analysis of cervical squamous cell carcinoma patients (n = 168) and their clinical and pathological characteristics including cytoplasmic HSP90 expression regarding PFS. Significant independent factors for PFS are indicated with asterisks. (* $p < 0.05$).

Covariate	Hazard Ratio	95% CI	*p*-Value
patient's age (<49 years vs. ≥49 years)	1.032	0.525–2.030	0.927
tumor grading	0.986	0.902–1.077	0.751
extent of the primary tumor [7]	2.104	1.096–4.038	0.025 *
nodal status (pNX/0 vs. pN1)	2.438	1.167–5.091	0.018 *
FIGO classification	0.496	0.259–0.950	0.034 *
positive cytoplasmic HSP90 expression	0.316	0.108–0.923	0.035 *

2.4. Correlation of Nuclear and Cytoplasmic HSP90 Expression with Histopathological Parameters

Nuclear and cytoplasmic HSP90 expression were correlated with the histopathological parameters previously published in the applied cervical cancer patient collective using Spearman's rank correlation coefficient (as shown in Table S1). Nuclear and cytoplasmic HSP90 expression were associated strongly with each other (Spearman rho: 0.422; $p < 0.001$) and with the expression of proteins that are important for necroptosis: Nuclear HSP90 expression was significantly correlated with nuclear RIPK1 (Spearman rho: 0.309; $p < 0.001$), cytoplasmic RIPK1 (Spearman rho: 0.410; $p < 0.001$), and nuclear RIPK3 (Spearman rho: 0.517; $p < 0.001$). Correspondingly, cytoplasmic HSP90 expression was also significantly associated with these proteins, showing correlations with nuclear RIPK1 (Spearman rho: 0.226; $p = 0.001$), cytoplasmic RIPK1 (Spearman rho: 0.426; $p < 0.001$), and nuclear RIPK3 (Spearman rho: 0.422; $p < 0.001$).

Cytoplasmic HSP90 expression was found to correlate positively with cytoplasmic E6 expression (Spearman rho: 0.138; $p = 0.042$). Additionally, nuclear p53 expression was associated with both nuclear (Spearman rho: 0.208; $p = 0.002$) and cytoplasmic HSP90 expression (Spearman rho: 0.254; $p < 0.001$). Similarly, p21 expression showed a positive correlation with both nuclear (Spearman rho: 0.229; $p = 0.002$) and cytoplasmic HSP90 expression (Spearman rho: 0.180; $p = 0.015$).

Nuclear HSP90 expression was found to positively correlate with the expression of mutated p53 (Spearman rho: 0.178; $p = 0.007$), nuclear LCoR (Spearman rho: 0.181; $p = 0.007$),

and glucocorticoid receptor (Spearman rho: 0.171; $p = 0.010$). Conversely, it negatively correlated with the expression of EP3 (Spearman rho: −0.192; $p = 0.004$), cytoplasmic H3K4me3 (Spearman rho: −0.215; $p = 0.001$), and MDM2 (Spearman rho: −0.156; $p = 0.022$).

Cytoplasmic HSP90 expression was positively associated with the expression of mutated p53 (Spearman rho: 0.176; $p = 0.008$), PRA in both the nucleus (Spearman rho: 0.155; $p = 0.020$) and cytoplasm (Spearman rho: 0.165; $p = 0.013$), as well as with cytoplasmic GPER (Spearman rho: 0.163; $p = 0.016$). In contrast, it was negatively associated with the expression of cytoplasmic p53 (Spearman rho: −0.150; $p = 0.025$) and mutated cytoplasmic p53 (Spearman rho: −0.205; $p = 0.002$).

3. Discussion

HSP90, expressed both in the nucleus and cytoplasm, plays diverse roles in cellular functions. In the nucleus, it is involved in modulating DNA structure, RNA synthesis and processing [23], and regulating transcription factors [24]. In the cytoplasm, HSP90 performs critical chaperone functions [25]. Its overexpression, which is currently under discussion for a potential role in tumorigenesis [26], has been associated with poor prognosis in cancers such as breast cancer [27,28] and colorectal cancer [29]. Consequently, HSP90 inhibitors have been explored in clinical trials for breast cancer [30,31]. Our study demonstrates that high nuclear HSP90 expression serves as an independent positive prognosticator in cervical squamous cell carcinoma. Furthermore, high cytoplasmic HSP90 expression correlates with improved PFS, lower FIGO classification, and a negative regional lymph node status (pN0). Given that HSP90 interacts with over 400 client proteins and is integral to numerous cellular pathways [32], its prognostic value could vary across different tumor entities.

In the context of cervical cancer, which is reliant on persistent hr-HPV infection [4], the viral oncoproteins E6 and E7 disrupt the cell cycle, promote immortalization, genomic instability, hyperproliferation, and inhibit apoptosis and necroptosis [5]. Previous research, including our own, has shown that the expression of necroptosis-relevant proteins (RIPK1, RIPK3) correlates with a better OS and PFS in cervical cancer patients [8]. These proteins are HSP90 clients, and inhibiting HSP90 leads to necroptosis suppression [19,33]. Our findings support this, showing a positive correlation between HSP90 expression and RIPK1 and RIPK3 in cervical cancer. While necroptosis is an undesirable mechanism in diseases like respiratory distress syndrome and chronic heart failure [34,35], in cervical cancer, it acts as a 'backup' mechanism, enabling infected cells to undergo regulated cell death, triggering immune responses, and potentially hindering the progression of hr-HPV-induced lesions [6]. This aligns with our key finding of a correlation between nuclear HSP90 overexpression and a better OS in cervical cancer patients.

In our study, correlations were observed between both nuclear and cytoplasmic HSP90 and nuclear p53 expression in cervical cancer, aligning with the known role of p53 as a client protein of HSP90 [36]. p53 functions as a tumor suppressor and is degraded by E6 in cervical cells with persistent hr-HPV infection [5]. Mutated p53 loses its tumor suppressor function and gains oncogenic properties [37]. The inhibition of HSP90 stabilizes mutated nuclear p53 in cancer cells [38], and HSP90 inhibitors have been shown to induce apoptosis in cervical cancer cell lines in vitro, albeit with limited efficacy in xenograft models [39]. The inhibition of HSP90 inhibits necroptosis [33]. This study's finding that high HSP90 expression correlates with better OS in cervical cancer may seem contradictory to the growth inhibition observed with HSP90 inhibitors in vitro. This discrepancy can be reconciled by considering necroptosis as a potential 'backup' cell death mechanism when apoptosis is inhibited [40]. High HSP90 expression might facilitate necroptosis in hr-HPV infected cells, negating carcinogenic effects, while HSP90 inhibitors induce apoptosis with tumor-suppressive outcomes.

Moreover, we observed a negative correlation between cytoplasmic HSP90 and cytoplasmic p53, which is known for its pro-apoptotic effects [41]. This supports the notion that cytoplasmic HSP90 overexpression could inhibit apoptosis while promoting necroptosis, due to its essential chaperone role for proteins involved in necroptosis [19–22,25]. These findings suggest a dual

role of HSP90 in programmed cell death: it appears to be anti-apoptotic on one hand, while potentially facilitating necroptosis on the other. Further experiments are warranted to explore these complex interactions and their implications for cervical cancer therapy.

In conclusion, our study reveals that high nuclear and cytoplasmic HSP90 expression serves as a positive prognostic indicator for OS and PFS, respectively, in patients with cervical squamous cell carcinoma. These findings underscore the dual role of HSP90 in modulating cell death pathways, particularly in the context of hr-HPV infection. The complex interplay between HSP90 and the proteins involved in apoptosis and necroptosis pathways highlights its potential as a biomarker and a therapeutic target in cervical cancer. Further research is warranted to fully understand HSP90's multifaceted role and to explore its implications in targeted cancer therapy.

4. Materials and Methods

4.1. Characteristics of Patients and Biopsies

In this study, we included all cervical cancer patients (n = 250) treated surgically at the Department of Gynecology and Obstetrics, Ludwig-Maximilians-University Munich, Germany, between 1993 and 2002, for whom paraffin-embedded carcinoma tissue was available, without any pre-selection. An experienced gynecological pathologist determined the histopathological tumor subtypes (squamous cell carcinoma, adenocarcinoma, adenosquamous carcinoma) and grading (G1: well differentiated, G2: moderately differentiated, G3: poorly differentiated). TNM classification (T = primary tumor site, N = regional lymph node involvement, M = presence of distant metastatic spread) was performed in accordance with the Union of International Cancer Control (UICC) guidelines, and the FIGO classification was assessed according to the Fédération Internationale de Gynécologie et d'Obstétrique (FIGO) criteria. Clinical and patient follow-up data were obtained from the Munich Cancer Registry (as presented in Table 3). The mean age of the patients at diagnosis was 49.0 ± 13.0 years, ranging from 20.4 to 83.3 years. Patients with an unknown cause of death or death unrelated to cervical cancer were censored. Correlation analyses with HSP90 expression were enabled by evaluating the other histopathological parameters in various previously published papers.

Table 3. Description of the clinical and pathological variables of the patients.

	Number of Cases (Total Number of Cases: n = 250)	%
Histopathological tumor subtype		
squamous cell carcinoma	194	77.6
adenocarcinoma	34	13.6
adenosquamous carcinoma	15	6.0
unknown	7	2.8
Tumor grading		
G1	21	8.4
G2	143	57.2
G3	78	31.2
unknown	8	3.2
Extent of primary tumor [7]		
pT1	107	42.8
pT2	126	50.4
pT3	9	3.6
pT4	1	0.4
unknown	7	2.8
Regional lymph node involvement (pN)		
pN0	145	58.0
pN1	98	39.2
unknown	7	2.8
Presence of distant metastatic spread (pM)		
pM0	2	0.8
pM1	7	2.8
pMX	235	94
unknown	6	2.4

Table 3. *Cont.*

	Number of Cases (Total Number of Cases: *n* = 250)	%
FIGO classification		
FIGO I	79	31.6
FIGO II	64	25.6
FIGO III	93	37.2
FIGO IV	7	2.8
unknown	7	2.8
Progression		
none	180	72.0
at least one	63	25.2
unknown	7	2.8
Survival		
censured	211	84.4
dead (tumor-dependent)	33	13.2
unknown	6	2.4

4.2. Immunohistochemistry

The cervical cancer tissue samples were fixed in 3.7% neutral buffered formalin immediately after resection, and then embedded in paraffin using standard procedures. Tissue microarrays (TMAs) were created from these formalin-fixed, paraffin-embedded tissues. For the immunohistochemical analysis, 3 µm tissue sections were first deparaffinized in Roticlear (Carl Roth GmbH + Co. KG, Karlsruhe, Germany) for 20 min, briefly washed in 100% ethanol, and then immersed in 3% H_2O_2 in methanol at room temperature for 20 min to inactivate the endogenous peroxidase. After rehydration through a descending ethanol gradient and a brief rinse in distilled water, the sections underwent epitope retrieval in a pressure cooker for 5 min using a sodium citrate buffer (pH 6.0; 0.1 mol/L citric acid/0.1 mol/L sodium citrate). Post retrieval, the slides were washed in distilled water and phosphate-buffered saline (PBS) twice for 2 min each. To block non-specific binding, Blocking Solution (ZytoChem Plus HRP Polymer System (Mouse/Rabbit); Zytomed Systems GmbH, Berlin, Germany) was applied for 5 min at room temperature. The sections were then incubated overnight at 4 °C with anti-HSP90 antibody (monoclonal mouse IgG, ab13492; Abcam, Cambridge, UK) diluted 1:1000 in PBS. This was followed by incubation with PostBlock Reagent and HRP-Polymer (Mouse/Rabbit) for 20 and 30 min, respectively, which contained secondary antibodies and peroxidase. After each incubation step, the slides were washed with PBS. For visualization, 3,3′-diaminobenzidine chromogen (DAB; Dako, Glostrup, Denmark) and its substrate buffer were applied for 30 s, and the reaction was halted by immersing the slides in distilled water. The tissue was counterstained with Mayer's acidic hematoxylin, dehydrated in an ascending ethanol gradient and Roticlear, and finally cover slipped with ROTI® Mount (Carl Roth GmbH + Co. KG, Karlsruhe, Germany). Fallopian tube tissue served as a positive control. Negative controls were processed by replacing primary antibodies with specific isotype control antibodies (BioGenex, Fremont, CA, USA).

4.3. Quantification

For the examination of the immunohistochemically stained cervical cancer slides, a Leitz Diaplan photomicroscope (Leitz, Wetzlar, Germany) was used. The staining of each specimen was quantified by the application of the semi-quantitative immunoreactive score (IRS), which is used for the optical evaluation of the intensity and distribution pattern of antigen expression [42]. The IRS was calculated by multiplying the number of positively stained cells (in %) (0: no staining; 1: 1–10% stained tumor cells; 2: 11–50% stained tumor cells; 3: 51–80% stained tumor cells; 4: >80% stained tumor cells) with the predominant staining intensity (0: none; 1: weak; 2: moderate; 3: strong). The scale goes from 0 (no expression) to 12 (very high expression). Images were taken with Flexacam C1 (Leica Microsystems (Switzerland) Ltd., Heerbrugg, Switzerland).

4.4. Statistical Analysis

IBM SPSS Statistics Version 26.0.0.0 (IBM, Armonk, New York, NY, USA) was used for data analysis. p-values of $p < 0.05$ were considered statistically significant. Group comparisons of independent groups regarding the clinical and pathological subgroups were tested with the Kruskal–Wallis–H test. Spearman's rank correlation coefficient was applied for the bivariate correlations between staining results in this study and the histopathological variables. The OS and PFS of the cervical cancer patients were tested for significance using the log-rank (Mantel-Cox) test and compared using Kaplan–Meier curves. A Cox regression model was established for a multivariate analysis of the investigated parameters. The variables included in the Cox regression model were the patient's age, histological subtype, tumor grading, TNM and FIGO classification, and HSP90 expression. HSP90 expression was divided into low and high expression for survival analysis. During analyses, the observers were fully blinded to the patients' data.

Supplementary Materials: The supporting information can be downloaded at: https://www.mdpi.com/article/10.3390/ijms25031571/s1.

Author Contributions: A.V. and U.J. designed and conceived the project, provided the concept, edited the manuscript, and supervised the research. T.L.R.V. performed all experiments, all statistical evaluation and wrote the manuscript. E.S., N.E.T., F.G. and S.M. contributed to the editing of the manuscript. All authors revised for critical intellectual content. All authors have read and agreed to the published version of the manuscript.

Funding: T.L.R.V. and A.V. have received funds for this study from the structured promotion program of Ludwig-Maximilians University of Munich, "Molecular and clinically translational Medicine" (Reg.-Nr. 27/2017).

Institutional Review Board Statement: The local ethics committee of Ludwig-Maximilians-University of Munich, Germany approved this study (approval number 259-16, 13 June 2016). All procedures involving human participants were in accordance with the ethical standards of the institutional and/or national research committee and with the Helsinki declaration of 1964 and its later amendments or comparable ethical standards. All tissue samples examined in this study were obtained from material from the archives of the Department of Gynecology and Obstetrics, Ludwig-Maximilians University of Munich. All diagnostic procedures were completed before the beginning of this study.

Informed Consent Statement: All patients gave informed consent prior to this study.

Data Availability Statement: Data are contained within the article.

Acknowledgments: The authors thank Christina Kuhn for her excellent technical assistance.

Conflicts of Interest: The authors declare no conflicts of interest. The funder (Ludwig-Maximilians University of Munich) has no role in the design of the study, in the collection, analyses, or interpretation of data, in the writing of the manuscript, or in the decision to publish the results.

Abbreviations

hr-HPV	high-risk human papillomavirus
RIPK3	receptor-interacting serine/threonine-protein kinase 3
MLKL	mixed lineage kinase domain-like protein
RIPK1	receptor-interacting serine/threonine-protein kinase 1
OS	overall survival
PFS	progression-free survival
HSP	heat shock protein
IRS	immunoreactive score
TMA	tissue microarray
PBS	phosphate buffer saline

References

1. World Health Organization. Cervical Cancer. Updated 20 January 2022. Available online: https://www.who.int/news-room/fact-sheets/detail/cervical-cancer (accessed on 17 November 2023).
2. Young, R.H.; Clement, P.B. Endocervical adenocarcinoma and its variants: Their morphology and differential diagnosis. *Histopathology* **2002**, *41*, 185–207. [CrossRef]
3. Leitlinienprogramm Onkologie (Deutsche Krebsgesellschaft, Deutsche Krebshilfe, AWMF): S3-Leitlinie Diagnostik, Therapie und Nachsorge der Patientin mit Zervixkarzinom, Langversion, 2.1, 2021, AWMF-Registernummer: 032/033OL. Available online: https://www.leitlinienprogramm-onkologie.de/leitlinien/zervixkarzinom/ (accessed on 25 February 2022).
4. Bosch, F.X.; Lorincz, A.; Muñoz, N.; Meijer, C.J.; Shah, K.V. The causal relation between human papillomavirus and cervical cancer. *J. Clin. Pathol.* **2002**, *55*, 244–265. [CrossRef]
5. Moody, C.A.; Laimins, L.A. Human papillomavirus oncoproteins: Pathways to transformation. *Nat. Rev. Cancer* **2010**, *10*, 550–560. [CrossRef] [PubMed]
6. MMa, W.; Tummers, B.; van Esch, E.M.; Goedemans, R.; Melief, C.J.; Meyers, C.; Boer, J.M.; van der Burg, S.H. Human Papillomavirus Downregulates the Expression of IFITM1 and RIPK3 to Escape from IFNγ- and TNFα-Mediated Antiproliferative Effects and Necroptosis. *Front. Immunol.* **2016**, *7*, 496. [CrossRef] [PubMed]
7. Galluzzi, L.; Vitale, I.; Aaronson, S.A.; Abrams, J.M.; Adam, D.; Agostinis, P.; Alnemri, E.S.; Altucci, L.; Amelio, I.; Andrews, D.W.; et al. Molecular mechanisms of cell death: Recommendations of the Nomenclature Committee on Cell Death 2018. *Cell Death Differ.* **2018**, *25*, 486–541. [CrossRef] [PubMed]
8. Vogelsang, T.L.R.; Kast, V.; Bagnjuk, K.; Eubler, K.; Jeevanandan, S.P.; Schmoeckel, E.; Trebo, A.; Topalov, N.E.; Mahner, S.; Mayr, D.; et al. RIPK1 and RIPK3 are positive prognosticators for cervical cancer patients and C2 ceramide can inhibit tumor cell proliferation in vitro. *Front. Oncol.* **2023**, *13*, 1110939. [CrossRef]
9. Zhang, X.; Zeng, Q.; Cai, W.; Ruan, W. Trends of cervical cancer at global, regional, and national level: Data from the Global Burden of Disease study 2019. *BMC Public Health* **2021**, *21*, 894. [CrossRef] [PubMed]
10. Drolet, M.; Bénard, É.; Pérez, N.; Brisson, M. Population-level impact and herd effects following the introduction of human papillomavirus vaccination programmes: Updated systematic review and meta-analysis. *Lancet* **2019**, *394*, 497–509. [CrossRef] [PubMed]
11. Atun, R.; Jaffray, D.A.; Barton, M.B.; Bray, F.; Baumann, M.; Vikram, B.; Hanna, T.P.; Knaul, F.M.; Lievens, Y.; Lui, T.Y.M.; et al. Expanding global access to radiotherapy. *Lancet Oncol.* **2015**, *16*, 1153–1186. [CrossRef] [PubMed]
12. Hartl, F.U.; Hayer-Hartl, M. Converging concepts of protein folding in vitro and in vivo. *Nat. Struct. Mol. Biol.* **2009**, *16*, 574–581. [CrossRef]
13. Saibil, H. Chaperone machines for protein folding, unfolding and disaggregation. *Nat. Rev. Mol. Cell Biol.* **2013**, *14*, 630–642. [CrossRef] [PubMed]
14. Schopf, F.H.; Biebl, M.M.; Buchner, J. The HSP90 chaperone machinery. *Nat. Rev. Mol. Cell Biol.* **2017**, *18*, 345–360. [CrossRef] [PubMed]
15. Hartl, F.U.; Bracher, A.; Hayer-Hartl, M. Molecular chaperones in protein folding and proteostasis. *Nature* **2011**, *475*, 324–332. [CrossRef] [PubMed]
16. Workman, P.; Burrows, F.; Neckers, L.; Rosen, N. Drugging the cancer chaperone HSP90: Combinatorial therapeutic exploitation of oncogene addiction and tumor stress. *Ann. N. Y. Acad. Sci.* **2007**, *1113*, 202–216. [CrossRef]
17. Jacobsen, A.V.; Silke, J. The importance of being chaperoned: HSP90 and necroptosis. *Cell Chem. Biol.* **2016**, *23*, 205–207. [CrossRef]
18. Li, D.; Xu, T.; Cao, Y.; Wang, H.; Li, L.; Chen, S.; Wang, X.; Shen, Z. A cytosolic heat shock protein 90 and cochaperone CDC37 complex is required for RIP3 activation during necroptosis. *Proc. Natl. Acad. Sci. USA* **2015**, *112*, 5017–5022. [CrossRef]
19. Li, D.; Li, C.; Li, L.; Chen, S.; Wang, L.; Li, Q.; Wang, X.; Lei, X.; Shen, Z. Natural Product Kongensin A is a Non-Canonical HSP90 Inhibitor that Blocks RIP3-dependent Necroptosis. *Cell Chem. Biol.* **2016**, *23*, 257–266. [CrossRef]
20. Lewis, J.; Devin, A.; Miller, A.; Lin, Y.; Rodriguez, Y.; Neckers, L.; Liu, Z.-G. Disruption of hsp90 function results in degradation of the death domain kinase, receptor-interacting protein (RIP), and blockage of tumor necrosis factor-induced nuclear factor-kappaB activation. *J. Biol. Chem.* **2000**, *275*, 10519–10526. [CrossRef]
21. Zhao, X.M.; Chen, Z.; Zhao, J.B.; Zhang, P.P.; Pu, Y.F.; Jiang, S.H.; Hou, J.J.; Cui, Y.M.; Jia, X.L.; Zhang, S.Q. Hsp90 modulates the stability of MLKL and is required for TNF-induced necroptosis. *Cell Death Dis.* **2016**, *7*, e2089. [CrossRef]
22. Jacobsen, A.V.; Lowes, K.N.; Tanzer, M.C.; Lucet, I.S.; Hildebrand, J.M.; Petrie, E.J.; van Delft, M.F.; Liu, Z.; A Conos, S.; Zhang, J.-G.; et al. HSP90 activity is required for MLKL oligomerisation and membrane translocation and the induction of necroptotic cell death. *Cell Death Dis.* **2016**, *7*, e2051. [CrossRef]
23. Hoter, A.; El-Sabban, M.E.; Naim, H.Y. The HSP90 Family: Structure, Regulation, Function, and Implications in Health and Disease. *Int. J. Mol. Sci.* **2018**, *19*, 2560. [CrossRef]
24. Calderwood, S.K.; Neckers, L. Hsp90 in Cancer: Transcriptional Roles in the Nucleus. *Adv. Cancer Res.* **2016**, *129*, 89–106.
25. Biebl, M.M.; Buchner, J. Structure, Function, and Regulation of the Hsp90 Machinery. *Cold Spring Harb. Perspect. Biol.* **2019**, *11*, a034017. [CrossRef]
26. Birbo, B.; Madu, E.E.; Madu, C.O.; Jain, A.; Lu, Y. Role of HSP90 in Cancer. *Int. J. Mol. Sci.* **2021**, *22*, 10317. [CrossRef] [PubMed]

27. Dimas, D.T.; Perlepe, C.D.; Sergentanis, T.N.; Misitzis, I.; Kontzoglou, K.; Patsouris, E.; Kouraklis, G.; Psaltopoulou, T.; Nonni, A. The Prognostic Significance of Hsp70/Hsp90 Expression in Breast Cancer: A Systematic Review and Meta-analysis. *Anticancer. Res.* **2018**, *38*, 1551–1562. [PubMed]
28. Cheng, Q.; Chang, J.T.; Geradts, J.; Neckers, L.M.; Haystead, T.; Spector, N.L.; Lyerly, H.K. Amplification and high-level expression of heat shock protein 90 marks aggressive phenotypes of human epidermal growth factor receptor 2 negative breast cancer. *Breast Cancer Res.* **2012**, *14*, R62. [CrossRef]
29. Zhang, S.; Guo, S.; Li, Z.; Li, D.; Zhan, Q. High expression of HSP90 is associated with poor prognosis in patients with colorectal cancer. *PeerJ* **2019**, *7*, e7946. [CrossRef] [PubMed]
30. Jhaveri, K.; Chandarlapaty, S.; Lake, D.; Gilewski, T.; Robson, M.; Goldfarb, S.; Drullinsky, P.; Sugarman, S.; Wasserheit-Leiblich, C.; Fasano, J.; et al. A phase II open-label study of ganetespib, a novel heat shock protein 90 inhibitor for patients with metastatic breast cancer. *Clin. Breast Cancer* **2014**, *14*, 154–160. [CrossRef] [PubMed]
31. Kong, A.; Rea, D.; Ahmed, S.; Beck, J.T.; López López, R.; Biganzoli, L.; Armstrong, A.C.; Aglietta, M.; Alba, E.; Campone, M.; et al. Phase 1B/2 study of the HSP90 inhibitor AUY922 plus trastuzumab in metastatic HER2-positive breast cancer patients who have progressed on trastuzumab-based regimen. *Oncotarget* **2016**, *7*, 37680–37692. [CrossRef] [PubMed]
32. Barrott, J.J.; Haystead, T.A. Hsp90, an unlikely ally in the war on cancer. *FEBS J.* **2013**, *280*, 1381–1396. [CrossRef] [PubMed]
33. Wu, Z.; Geng, Y.; Lu, X.; Shi, Y.; Wu, G.; Zhang, M.; Shan, B.; Pan, H.; Yuan, J. Chaperone-mediated autophagy is involved in the execution of ferroptosis. *Proc. Natl. Acad. Sci. USA* **2019**, *116*, 2996–3005. [CrossRef]
34. Yu, X.; Mao, M.; Liu, X.; Shen, T.; Li, T.; Yu, H.; Zhang, J.; Chen, X.; Zhao, X.; Zhu, D. A cytosolic heat shock protein 90 and co-chaperone p23 complex activates RIPK3/MLKL during necroptosis of endothelial cells in acute respiratory distress syndrome. *J. Mol. Med.* **2020**, *98*, 569–583. [CrossRef]
35. Marunouchi, T.; Nishiumi, C.; Iinuma, S.; Yano, E.; Tanonaka, K. Effects of Hsp90 inhibitor on the RIP1-RIP3-MLKL pathway during the development of heart failure in mice. *Eur. J. Pharmacol.* **2021**, *898*, 173987. [CrossRef]
36. Walerych, D.; Kudla, G.; Gutkowska, M.; Wawrzynow, B.; Muller, L.; King, F.W.; Helwak, A.; Boros, J.; Zylicz, A.; Zylicz, M. Hsp90 chaperones wild-type p53 tumor suppressor protein. *J. Biol. Chem.* **2004**, *279*, 48836–48845. [CrossRef] [PubMed]
37. Chen, X.; Zhang, T.; Su, W.; Dou, Z.; Zhao, D.; Jin, X.; Lei, H.; Wang, J.; Xie, X.; Cheng, B.; et al. Mutant p53 in cancer: From molecular mechanism to therapeutic modulation. *Cell Death Dis.* **2022**, *13*, 974. [CrossRef] [PubMed]
38. Li, D.; Marchenko, N.D.; Schulz, R.; Fischer, V.; Velasco-Hernandez, T.; Talos, F.; Moll, U.M. Functional inactivation of endogenous MDM2 and CHIP by HSP90 causes aberrant stabilization of mutant p53 in human cancer cells. *Mol. Cancer Res.* **2011**, *9*, 577–588. [CrossRef] [PubMed]
39. Schwock, J.; Pham, N.A.; Cao, M.P.; Hedley, D.W. Efficacy of Hsp90 inhibition for induction of apoptosis and inhibition of growth in cervical carcinoma cells in vitro and in vivo. *Cancer Chemother. Pharmacol.* **2008**, *61*, 669–681. [CrossRef] [PubMed]
40. Tummers, B.; Green, D.R. The evolution of regulated cell death pathways in animals and their evasion by pathogens. *Physiol. Rev.* **2022**, *102*, 411–454. [CrossRef] [PubMed]
41. Green, D.R.; Kroemer, G. Cytoplasmic functions of the tumour suppressor p53. *Nature* **2009**, *458*, 1127–1130. [CrossRef] [PubMed]
42. Remmele, W.; Stegner, H.E. Recommendation for uniform definition of an immunoreactive score (IRS) for immunohistochemical estrogen receptor detection (ER-ICA) in breast cancer tissue. *Pathologe* **1987**, *8*, 138–140.

7. Literaturverzeichnis

1. Remmele W, Stegner HE. [Recommendation for uniform definition of an immunoreactive score (IRS) for immunohistochemical estrogen receptor detection (ER-ICA) in breast cancer tissue]. Pathologe. 1987;8(3):138-40.

2. World Health Organization. Cervical cancer [updated 05.03.2024. Available from: https://www.who.int/news-room/fact-sheets/detail/cervical-cancer, abgerufen am: 28.09.2024].

3. Leitlinienprogramm Onkologie (Deutsche Krebsgesellschaft, Deutsche Krebshilfe, AWMF): S3-Leitlinie Diagnostik, Therapie und Nachsorge der Patientin mit Zervixkarzinom, Langversion, 2.2, 2022, AWMF-Registernummer: 032/033OL [Available from: https://www.leitlinienprogramm-onkologie.de/leitlinien/zervixkarzinom, abgerufen am: 28.09.2024].

4. Vogelsang TLR, Kast V, Bagnjuk K, Eubler K, Jeevanandan SP, Schmoeckel E, et al. RIPK1 and RIPK3 are positive prognosticators for cervical cancer patients and C2 ceramide can inhibit tumor cell proliferation in vitro. Front Oncol. 2023;13:1110939.

5. Zhang X, Zeng Q, Cai W, Ruan W. Trends of cervical cancer at global, regional, and national level: data from the Global Burden of Disease study 2019. BMC Public Health. 2021;21(1):894.

6. Vogelsang TLR, Schmoeckel E, Topalov NE, Ganster F, Mahner S, Jeschke U, et al. Prognostic Impact of Heat Shock Protein 90 Expression in Women Diagnosed with Cervical Cancer. Int J Mol Sci. 2024;25(3).

7. Brisson M, Kim JJ, Canfell K, Drolet M, Gingras G, Burger EA, et al. Impact of HPV vaccination and cervical screening on cervical cancer elimination: a comparative modelling analysis in 78 low-income and lower-middle-income countries. Lancet. 2020;395(10224):575-90.

8. Arbyn M, Weiderpass E, Bruni L, de Sanjosé S, Saraiya M, Ferlay J, et al. Estimates of incidence and mortality of cervical cancer in 2018: a worldwide analysis. Lancet Glob Health. 2020;8(2):e191-e203.

9. Krebs in Deutschland für 2019/2020. 14.Ausgabe. Robert Koch-Institut (Hrsg.) und die Gesellschaft der epidemiologischen Krebsregister in Deutschland e.V. (Hrsg.). Berlin, 2023 [Available from: https://www.krebsdaten.de/Krebs/DE/Content/Publikationen/Krebs_in_Deutschland/krebs_in_deutschland_2023.pdf?__blob=publicationFile, abgerufen am: 28.09.2024].

10. Bosch FX, Lorincz A, Muñoz N, Meijer CJ, Shah KV. The causal relation between human papillomavirus and cervical cancer. J Clin Pathol. 2002;55(4):244-65.

11. Lee JE, Chung Y, Rhee S, Kim TH. Untold story of human cervical cancers: HPV-negative cervical cancer. BMB Rep. 2022;55(9):429-38.

12. Schiffman M, Wentzensen N, Wacholder S, Kinney W, Gage JC, Castle PE. Human papillomavirus testing in the prevention of cervical cancer. J Natl Cancer Inst. 2011;103(5):368-83.

13. Moody CA, Laimins LA. Human papillomavirus oncoproteins: pathways to transformation. Nature Reviews Cancer. 2010;10(8):550-60.

14. Grando SA. Connections of nicotine to cancer. Nature Reviews Cancer. 2014;14(6):419-29.

15. Cibula D, Raspollini MR, Planchamp F, Centeno C, Chargari C, Felix A, et al. ESGO/ESTRO/ESP Guidelines for the management of patients with cervical cancer - Update 2023. Int J Gynecol Cancer. 2023;33(5):649-66.

16. Maguire FB, Cooley JJP, Morris CR, Parikh-Patel A, Kennedy VA, Keegan THM. Symptomatic presentation of cervical cancer in emergency departments in California. Cancer Causes Control. 2021;32(12):1411-21.

17. Arbeitsgemeinschaft fuïr gynäkologische Onkologie (AGO) der Österreichischen Gesellschaft fuïr Gynäkologie und Geburtshilfe (OEGGG) CG, Christian Schauer. Manual der gynäkologischen Onkologie 2023 [Available from: https://ago-austria.at/zervixkarzinom-diagnostik/, abgerufen am: 28.09.2024].

18. Wittekind C, Bootz F, Meyer HJ. Gynäkologische Tumoren. In: Wittekind C, Bootz F, Meyer HJ, editors. TNM Klassifikation maligner Tumoren. Berlin, Heidelberg: Springer Berlin Heidelberg; 2004. p. 131-65.

19. Piver MS, Rutledge F, Smith JP. Five classes of extended hysterectomy for women with cervical cancer. Obstet Gynecol. 1974;44(2):265-72.

20. Koch-Institut R. Epidemiologisches Bulletin 12 / 2007. Robert Koch-Institut; 2007. p. 97-103.

21. Koch-Institut R. Epidemiologisches Bulletin 34 / 2018. 2018:335, 47-48.

22. Lei J, Ploner A, Elfström KM, Wang J, Roth A, Fang F, et al. HPV Vaccination and the Risk of Invasive Cervical Cancer. N Engl J Med. 2020;383(14):1340-8.

23. Koch-Institut R. Epidemiologisches Bulletin 36 / 2022. 2022:11-22.

24. Falcaro M, Castañon A, Ndlela B, Checchi M, Soldan K, Lopez-Bernal J, et al. The effects of the national HPV vaccination programme in England, UK, on cervical cancer and grade 3 cervical intraepithelial neoplasia incidence: a register-based observational study. Lancet. 2021;398(10316):2084-92.

25. Paavonen J, Naud P, Salmerón J, Wheeler CM, Chow SN, Apter D, et al. Efficacy of human papillomavirus (HPV)-16/18 AS04-adjuvanted vaccine against cervical infection and precancer caused by oncogenic HPV types (PATRICIA): final analysis of a double-blind, randomised study in young women. Lancet. 2009;374(9686):301-14.

26. Joura EA, Giuliano AR, Iversen OE, Bouchard C, Mao C, Mehlsen J, et al. A 9-valent HPV vaccine against infection and intraepithelial neoplasia in women. N Engl J Med. 2015;372(8):711-23.

27. Kerr JF, Wyllie AH, Currie AR. Apoptosis: a basic biological phenomenon with wide-ranging implications in tissue kinetics. Br J Cancer. 1972;26(4):239-57.

28. Jorgensen I, Rayamajhi M, Miao EA. Programmed cell death as a defence against infection. Nat Rev Immunol. 2017;17(3):151-64.

29. Dyson N, Howley PM, Münger K, Harlow E. The human papilloma virus-16 E7 oncoprotein is able to bind to the retinoblastoma gene product. Science. 1989;243(4893):934-7.

30. Chellappan S, Kraus VB, Kroger B, Munger K, Howley PM, Phelps WC, et al. Adenovirus E1A, simian virus 40 tumor antigen, and human papillomavirus E7 protein share the capacity to disrupt the interaction between transcription factor E2F and the retinoblastoma gene product. Proc Natl Acad Sci U S A. 1992;89(10):4549-53.

31. Scheffner M, Werness BA, Huibregtse JM, Levine AJ, Howley PM. The E6 oncoprotein encoded by human papillomavirus types 16 and 18 promotes the degradation of p53. Cell. 1990;63(6):1129-36.

32. Martinez-Zapien D, Ruiz FX, Poirson J, Mitschler A, Ramirez J, Forster A, et al. Structure of the E6/E6AP/p53 complex required for HPV-mediated degradation of p53. Nature. 2016;529(7587):541-5.

33. Scheffner M, Huibregtse JM, Vierstra RD, Howley PM. The HPV-16 E6 and E6-AP complex functions as a ubiquitin-protein ligase in the ubiquitination of p53. Cell. 1993;75(3):495-505.

34. Upton JW, Kaiser WJ, Mocarski ES. DAI/ZBP1/DLM-1 complexes with RIP3 to mediate virus-induced programmed necrosis that is targeted by murine cytomegalovirus vIRA. Cell Host Microbe. 2012;11(3):290-7.

35. Sun L, Wang H, Wang Z, He S, Chen S, Liao D, et al. Mixed lineage kinase domain-like protein mediates necrosis signaling downstream of RIP3 kinase. Cell. 2012;148(1-2):213-27.

36. Kaiser WJ, Upton JW, Mocarski ES. Viral modulation of programmed necrosis. Curr Opin Virol. 2013;3(3):296-306.

37. Wang H, Sun L, Su L, Rizo J, Liu L, Wang LF, et al. Mixed lineage kinase domain-like protein MLKL causes necrotic membrane disruption upon phosphorylation by RIP3. Mol Cell. 2014;54(1):133-46.

38. Kaczmarek A, Vandenabeele P, Krysko DV. Necroptosis: the release of damage-associated molecular patterns and its physiological relevance. Immunity. 2013;38(2):209-23.

39. Bertrand MJ, Milutinovic S, Dickson KM, Ho WC, Boudreault A, Durkin J, et al. cIAP1 and cIAP2 facilitate cancer cell survival by functioning as E3 ligases that promote RIP1 ubiquitination. Mol Cell. 2008;30(6):689-700.

40. Vanlangenakker N, Bertrand MJ, Bogaert P, Vandenabeele P, Vanden Berghe T. TNF-induced necroptosis in L929 cells is tightly regulated by multiple TNFR1 complex I and II members. Cell Death Dis. 2011;2(11):e230.

41. Micheau O, Lens S, Gaide O, Alevizopoulos K, Tschopp J. NF-kappaB signals induce the expression of c-FLIP. Mol Cell Biol. 2001;21(16):5299-305.

42. Vanden Berghe T, Linkermann A, Jouan-Lanhouet S, Walczak H, Vandenabeele P. Regulated necrosis: the expanding network of non-apoptotic cell death pathways. Nat Rev Mol Cell Biol. 2014;15(2):135-47.

43. Irmler M, Thome M, Hahne M, Schneider P, Hofmann K, Steiner V, et al. Inhibition of death receptor signals by cellular FLIP. Nature. 1997;388(6638):190-5.

44. Oberst A, Dillon CP, Weinlich R, McCormick LL, Fitzgerald P, Pop C, et al. Catalytic activity of the caspase-8-FLIP(L) complex inhibits RIPK3-dependent necrosis. Nature. 2011;471(7338):363-7.

45. Lin Y, Devin A, Rodriguez Y, Liu ZG. Cleavage of the death domain kinase RIP by caspase-8 prompts TNF-induced apoptosis. Genes Dev. 1999;13(19):2514-26.

46. O'Donnell MA, Perez-Jimenez E, Oberst A, Ng A, Massoumi R, Xavier R, et al. Caspase 8 inhibits programmed necrosis by processing CYLD. Nat Cell Biol. 2011;13(12):1437-42.

47. Mocarski ES, Upton JW, Kaiser WJ. Viral infection and the evolution of caspase 8-regulated apoptotic and necrotic death pathways. Nat Rev Immunol. 2011;12(2):79-88.

48. Vanden Berghe T, Hassannia B, Vandenabeele P. An outline of necrosome triggers. Cell Mol Life Sci. 2016;73(11-12):2137-52.

49. Moquin DM, McQuade T, Chan FK. CYLD deubiquitinates RIP1 in the TNFα-induced necrosome to facilitate kinase activation and programmed necrosis. PLoS One. 2013;8(10):e76841.

50. Hannun YA, Obeid LM. Sphingolipids and their metabolism in physiology and disease. Nat Rev Mol Cell Biol. 2018;19(3):175-91.

51. Ogretmen B, Hannun YA. Biologically active sphingolipids in cancer pathogenesis and treatment. Nature Reviews Cancer. 2004;4(8):604-16.

52. Bieberich E, Kawaguchi T, Yu RK. N-acylated serinol is a novel ceramide mimic inducing apoptosis in neuroblastoma cells. J Biol Chem. 2000;275(1):177-81.

53. Struckhoff AP, Bittman R, Burow ME, Clejan S, Elliott S, Hammond T, et al. Novel ceramide analogs as potential chemotherapeutic agents in breast cancer. J Pharmacol Exp Ther. 2004;309(2):523-32.

54. Bagnjuk K, Stöckl JB, Fröhlich T, Arnold GJ, Behr R, Berg U, et al. Necroptosis in primate luteolysis: a role for ceramide. Cell Death Discov. 2019;5:67.

55. Li D, Xu T, Cao Y, Wang H, Li L, Chen S, et al. A cytosolic heat shock protein 90 and cochaperone CDC37 complex is required for RIP3 activation during necroptosis. Proc Natl Acad Sci U S A. 2015;112(16):5017-22.

56. Li D, Li C, Li L, Chen S, Wang L, Li Q, et al. Natural Product Kongensin A is a Non-Canonical HSP90 Inhibitor that Blocks RIP3-dependent Necroptosis. Cell Chem Biol. 2016;23(2):257-66.

57. Lewis J, Devin A, Miller A, Lin Y, Rodriguez Y, Neckers L, et al. Disruption of hsp90 function results in degradation of the death domain kinase, receptor-interacting protein (RIP), and blockage of tumor necrosis factor-induced nuclear factor-kappaB activation. J Biol Chem. 2000;275(14):10519-26.

58. Zhao XM, Chen Z, Zhao JB, Zhang PP, Pu YF, Jiang SH, et al. Hsp90 modulates the stability of MLKL and is required for TNF-induced necroptosis. Cell Death & Disease. 2016;7(2):e2089-e.

59. Jacobsen AV, Lowes KN, Tanzer MC, Lucet IS, Hildebrand JM, Petrie EJ, et al. HSP90 activity is required for MLKL oligomerisation and membrane translocation and the induction of necroptotic cell death. Cell Death Dis. 2016;7(1):e2051.

60. Hartl FU, Bracher A, Hayer-Hartl M. Molecular chaperones in protein folding and proteostasis. Nature. 2011;475(7356):324-32.

61. Schopf FH, Biebl MM, Buchner J. The HSP90 chaperone machinery. Nat Rev Mol Cell Biol. 2017;18(6):345-60.

62. Jacobsen AV, Silke J. The importance of being chaperoned: HSP90 and necroptosis. Cell Chem Biol. 2016;23(2):205-7.

63. Ma W, Tummers B, van Esch EM, Goedemans R, Melief CJ, Meyers C, et al. Human Papillomavirus Downregulates the Expression of IFITM1 and RIPK3 to Escape from IFNγ- and TNFα-Mediated Antiproliferative Effects and Necroptosis. Front Immunol. 2016;7:496.

Danksagung

Ich danke meinem Doktorvater Udo Jeschke, der mich stets unterstützt, gefördert und mir das Interesse und die Liebe zum wissenschaftlichen Arbeiten nähergebracht hat. *„Man muss in den Erfolg verliebt sein, und nicht ins Scheitern“* ist nur eines der vielen motivierenden Zitate, welche mich zu Bestleistungen brachte. Nach wie vor beeindruckt mich die durch Udo Jeschke perfektionierte Kombination aus Professionalität und Empathie, durch die man sich zu jeder Zeit wertgeschätzt und verstanden fühlt.

Ein großer Dank gebührt Aurelia Vattai, für ihre Unterstützung, das Erwecken meines Interesses am Fach der Frauenheilkunde und Geburtshilfe sowie die wertschätzende, fachliche Betreuung.

Ganz besonders möchte ich dem Laborteam der Maistraße danken, allen voran Christina Kuhn, Simone Hofmann und Martina Rahmeh. Ihr habt die Arbeit im Labor nicht nur erleichtert, sondern seid eine unglaubliche Bereicherung.

Ich bin sehr dankbar für all die Freundschaften, die im Rahmen der Doktorarbeit entstanden sind. Ganz besonders hervorheben möchte ich Nicole, die mich durch ihre Motivation und fachliche Kompetenz nachhaltig beeindruckt hat, die immer ein offenes Ohr hat und mit der ich viele Höhen und Tiefen teilen durfte. Vielen Dank an Jule, Nadine, Anna Trebo, Anna Buchholz und Mareike, ohne die die Arbeit im Labor nicht so schön und lustig gewesen wäre. Gemeinsam gelang es uns, aus belastenden Situationen einen Funken Komik zu gewinnen und uns gegenseitig den Alltag im Labor zu erleichtern.

Vielen Dank an Prof. Mayerhofer und sein Team (Konstantin, Verena, Katja, Sree, Carola und Michelle) für die hervorragende Zusammenarbeit.

Ich danke Prof. Waschke, der mich motiviert hat, mich um eine experimentelle Doktorarbeit zu bemühen. Er hat den Anstoß geliefert, mich für das strukturierte Promotionsprogramm FöFoLe zu bewerben.

Ich danke meiner Partnerin Joana, die mir auch bei Rückschlägen zur Seite stand, Verständnis für meine Verstimmungen nach langen Labortagen entgegenbrachte, ihre Liebe und ihre nicht enden wollende Unterstützung.

Mein größter Dank gilt meiner Mama, meinem Papa, Linus, Lennart, Omama, Mutti und Großvater. Eure ungebrochene Unterstützung, Liebe und Ehrlichkeit haben es mir ermöglicht, den Weg des Medizinstudiums sowie dieser Dissertation zu gehen. Ohne euch wäre nichts hiervon möglich gewesen.